Research Square

Preprints are preliminary reports that have not undergone peer review.
They should not be considered conclusive, used to inform clinical practice,
or referenced by the media as validated information.

Minigene-based characterization and classification of splice-associated variants in succinate dehydrogenase B

Anni Köhler
University Hospital Carl Gustav Carus at TUD Dresden University of Technology, Dresden University of Technology
Alexandra A. Baumann
University Hospital Carl Gustav Carus at TUD Dresden University of Technology, Dresden University of Technology
Natasha Lewis
University Hospital Carl Gustav Carus at TUD Dresden University of Technology, Dresden University of Technology
Anja Richter
University Hospital Carl Gustav Carus at TUD Dresden University of Technology, Dresden University of Technology
Susan Richter
University of Auckland
Doreen William
University Hospital Carl Gustav Carus at TUD Dresden University of Technology, Dresden University of Technology
Andrés Cruz Garcia
Nationales Centrum für Tumorerkrankungen Dresden
Hanno Glimm
DKTK, Partner Site Dresden
Stefan Fröhling
German Cancer Research Center
Diana Le Duc
University Hospital Carl Gustav Carus at TUD Dresden University of Technology, Dresden University of Technology
Evelin Schröck
University Hospital Carl Gustav Carus at TUD Dresden University of Technology, Dresden University of Technology
Arne Jahn
Arne.Jahn@ukdd.de

University Hospital Carl Gustav Carus at TUD Dresden University of Technology, Dresden University of Technology

Article

Keywords: mini-gene assay, splicing, ACMG, PVS1_RNA, variant classification, precision medicine

Posted Date: February 24th, 2026

DOI: https://doi.org/10.21203/rs.3.rs-8661010/v1

License: This work is licensed under a Creative Commons Attribution 4.0 International License. Read Full License

Additional Declarations: Competing interest reported. S.F.: Honoraria: Illumina. E.S.: Honoraria: Illumina. A.J.: Honoraria: AstraZeneca. The other authors declare no competing interests.

Version of Record: A version of this preprint was published at npj Precision Oncology on September 8th, 2026. See the published version at https://doi.org/10.1038/s41698-026-01685-7.

Abstract

Pathogenic germline variants in SDHB are associated with an increased risk for tumors such as pheochromocytoma and paraganglioma. However, limited functional evidence for rare variants poses a major challenge for clinical decision making. To systematically investigate potentially splice-associated variants of unknown significance (VUS) in SDHB, we created a minigene spanning exons 2-5 and assessed minigene-derived SDHB transcripts in HEK293T cells using targeted NGS analysis. We characterized the transcriptional impact of 48 variants prioritized by SpliceAI (Δ ≥ 0.42), along with two negative controls as well as endogenous SDHB, and compared effects with primary cancer data (n=2). While 19 variants (38%) showed ≥90% wildtype expression, 17 variants (34%) exhibited ≥90% aberrant splicing. Across all variants, an average of 2.3 transcripts per variant was detected, yielding a total of 113 transcripts. Applying a customized PVS1/BP7 decision tree, weighted transcript strengths could be assigned to 104 transcripts (92%). For a total of 26 classified variants, this yielded a PVS1_Strong (RNA) code for 10 variants (38%), including eight canonical splice-site variants, one missense variant and one stop-gain variant, a PVS1_Moderate (RNA) code for two non-canonical intronic variants (8%), and a BP7_Strong (RNA) code for 14 intronic or synonymous variants (54%). Integration of minigene RNA data resulted in an average ACMG point change (Δ) of 2.7 (median Δ = 3.5; range: 1–4), with an increase for three variants (11.5%) and a decrease for 23 variants (88.5%). Reclassification occurred in 13 variants (50%), with 12 variants downgraded from VUS to likely benign, and one variant (c.402T>A) downgraded from likely pathogenic to VUS. We conclude that targeted RNA sequencing of minigene derived transcripts represents a precise and scalable approach for assessing splice-associated variants for precision oncology. Nevertheless, RNA-based evidence should be interpreted in the context of complementary functional and clinical data to ensure robust variant classification.

Introduction

Genetic testing is increasingly used in precision oncology to identify targetable vulnerabilities of tumors or individuals with hereditary cancer, but the functional classification of genetic variants remains challenging. Succinate dehydrogenase [ubiquinone] iron-sulfur subunit (*SDHB*) is a core component of the SDH complex or complex II, which uniquely links the tricarboxylic acid (TCA) cycle and the electron transport chain. Pathogenic loss-of-function germline variants in *SDHB* and other tumor suppressor genes are observed in 24%-44% of individuals with paraganglioma or pheochromocytoma (PPGL), rare tumors derived from neuroendocrine tissues. In addition to PPGLs, the risks for other cancers, such as gastrointestinal stromal tumors and renal cell carcinoma are increased in hereditary PPGL syndrome (Amar et al., 2005; Burnichon et al., 2009; Fassnacht et al., 2018). Moreover, *SDHB*-associated hereditary PPGL syndrome is frequently associated with aggressive disease behavior and poor clinical outcomes, underscoring the clinical importance of accurate and timely variant interpretation.

Approximately 40% of *SDHB* variants are currently classified as variants of uncertain significance (VUS) in the ClinVar database (Landrum et al., 2014), highlighting a substantial gap for clinical decision making. To address this challenge, current efforts to improve classifications for endocrine tumor predisposition variants (ENDO-TPS VCEP), including *SDHB*, are ongoing and coordinated by the Clinical Genome Resource (ClinGen (Rehm et al., 2015)). Nevertheless, reliable assessment of pathogenicity, especially for intronic and synonymous variants, is a non-trivial task and typically lead to a classification as VUS according to ACMG/AMP criteria (Richards et al., 2015), as functional readouts and patient samples are rarely available. Although *in-silico* tools, such as SpliceAI (Jaganathan et al., 2019) can help identify and prioritize potentially splice-disrupting variants, these predictions must be complemented by experimental assays. With the continuous expansion of genetic testing increasing the numbers of variants, there is a growing need for scalable approaches capable of classifying large numbers of variants.

One well-established and streamlined assay to interrogate splice-associated variants is the minigene assay, which investigates the impact of genetic variants on pre-mRNA splicing. By cloning genomic fragments covering the exon(s) of interest and their flanking intronic sequences into a plasmid, variant-induced splicing changes can be directly assessed in a controlled cellular context. Minigene assays have been successfully applied to tumor suppressor genes such as *CHEK2, RAD51C, BRCA1, BRCA2, TP53, MLH1, MSH2, MSH6*, and *PMS2* (Canson et al., 2025; Dong et al., 2023; Fraile-Bethencourt et al., 2019; Sanoguera-Miralles et al., 2022, 2024; van der Klift et al., 2015), thereby improving variant classification and clinical translation.

In this study, we established and validated an *SDHB* minigene to systematically assess the impact on splicing of 48 variants located in exon 3, 4, and adjacent intronic regions. Variants were prioritized with SpliceAI (Jaganathan et al., 2019) and a targeted NGS-based workflow was implemented to enable precise identification, characterization and quantification of splice isoforms. Additionally, we integrated RNA-based insights into an *SDHB*-adapted ACMG/AMP framework to support variant reclassification. Together, this approach provides a quantitative and scalable strategy to improve classification of splice-associated variants in *SDHB*.

Material and Methods

Reference sequences and nomenclature

All genomic coordinates refer to the hg38/GRCh38 reference genome. Coding positions correspond to the *SDHB* MANE Select transcript (NM_003000.3 / ENST00000375499.8), as defined by the Matched Annotation from NCBI and EMBL-EBI (MANE) project (Morales et al., 2022) and amino acid positions refer to the SDHB protein reference NP_002991.2 (*SDHB* gene – Gene ID: 6390) and UniProt P21912 (The UniProt Consortium). Variant nomenclature follows HGVS recommendations (Hart et al., 2024a). The plasmid sequence of the *SDHB* minigene is described in Supp. Mat. 1.1/1.2 and reference files are available in GitHub (GitHub/*SDHB*_minigene/04_Minigene_Reference).

Public transcript expression data from the Genotype-Tissue Expression (GTEx, (GTEx Consortium, 2020)) project were consulted to assess the tissue-wide expression of annotated *SDHB* transcript isoforms. Data were accessed via the GTEx Portal (https://gtexportal.org).

Variant selection / Bioinformatic analysis

We selected the genomic region for experimental assessment of splice-associated *SDHB* variants based on functional considerations. Specifically, we included exons 2–5 and their flanking intronic sequences as they encompass essential protein domains and contain out-of-frame exon lengths. We systematically generated all possible single-nucleotide variants (SNVs) (GitHub/*SDHB*_minigene/01_Synthetic_Variant_Table) across the selected *SDHB* region and annotated them using the Ensembl Variant Effect Predictor (VEP; accessed 30.06.2023; GitHub/*SDHB*_minigene/03_Variant_Prioritization). Splice-associated variants were predicted with the *in-silico* prediction tool SpliceAI (raw REF/ALT VCF mode) which provides Δ-scores for donor and acceptor loss or gain (GitHub/*SDHB*_minigene/02_SpliceAI_Run). We used a permissive maximum delta score ≥ 0.25 to maximize sensitivity for detecting potential splice-altering variants (Jaganathan et al., 2019). From the resulting dataset, 48 splice-associated variants were selected (GitHub/*SDHB*_minigene/03_Variant_Prioritization) for subsequent experimental assessment, ensuring representation of canonical splice-sites as well as exonic and intronic positions.

Minigene cloning and mutagenesis

The *SDHB* minigene was designed using the NEBuilder Assembly Tool and cloned into a linearized pcDNA3.1/Hygro(-) backbone (5596 nt) (Supp. Mat. 1.1) under the control of a CMV promoter (Addgene plasmid V875-20). Exons 2–5 (A1-A3; 2905 nt. total length) together with their flanking intronic regions (Supp. Mat. 1.2) were amplified from 100 ng genomic DNA from HEK293T and human blood (Supp. Figure 1).

Amplicon	Genomic region (hg38)	Length	Content	Reference genome	Template DNA
A1	chr1:17,044,436 – 17,045,090	639 bp	202bp intron 1, 128bp exon 2, 325bp intron 2	Hg 38	Human blood (gDNA)
A2	chr1:17,032,736 – 17,033,470	759 bp	325bp intron 2, 86bp exon 3, 325bp intron 3	Chr1_MU27333v1_fix (Hg38 fix) 1-17033181-G-T (C-A)	HEK293T (gDNA)
A3	chr1:17,027,547 – 17,029,061	1553 bp	325bp intron 3, 137bp exon 4, 734bp intron 4, 117bp exon 5, 202bp intron 5	Chr1_MU27333v1_fix (Hg38 fix) 1-17028892-A-G (T-C)	HEK293T (gDNA)

Methods Table 1. Amplicon design and genomic content of *SDHB* minigene constructs. Genomic coordinates (GRCh38/hg38), amplicon lengths and exon-intron composition of the three *SDHB* amplicons used for minigene cloning are listed. For each amplicon, the reference genome and the source of template DNA are indicated.

Amplicons were generated from 100 ng of template DNA in 50 µL reactions using Q5® High-Fidelity DNA Polymerase (NEB, M0491). Each reaction contained 1× Q5 Reaction Buffer, 1× Q5 High GC Enhancer, Q5 High-Fidelity DNA Polymerase (1U), 10 mM dNTPs (1 µl) and 2.5 µL of 10 µM *SDHB*-specific forward and reverse primers (≥ 20 nt; metabion; Supp. Mat. 1.3). Primers included non-priming 5' overhangs (≥ 25 bp) homologous to the 5'-terminal sequence of the adjacent amplicon and a gene specific 3' region. PCR cycling conditions were: denaturation at 98°C for 30 s; 30 cycles of 98°C for 30 s, annealing at primer Tm (58–67°C) for 45 s, and extension at 72°C for 1 min; followed by final extension at 72°C for 10 min. The vector backbone was digested with BamHI-HF / XhoI (NEB, R3136S / R0146S) at 37°C for 1h. Sticky-end fragments were assembled using the NEBuilder HiFi DNA Assembly Cloning Kit (M5520G) at a 2:1 insert to vector ratio and incubation of reaction at 50°C for 60 min. Assembled plasmids (8441 bp) were transformed into chemically competent *E.coli* DH5α cells (NEB, C29871) by heat shock (42°C, 45 s), followed by recovery in LB medium for 30 min. at 37°C and selection on ampicillin agar plates (100 µg/ml). Inserts were screened by colony PCR using primers: MG_Val_Fwd and MG_Val_Rev (Supp. Mat. 1.3), followed by agarose gel electrophoresis (1% agarose, 1 h 15 min, expected amplicon size 3029 bp). Selected clones were purified using plasmid Miniprep Kit (Qiagen, 27106) and minigene plasmid sequence was validated by next-generation sequencing (Illumina DNA Prep Flex; NextSeq 2000).

Variants were introduced into the minigene using site directed mutagenesis, performed with a QuikChange-style protocol with modified primer design (Zheng et al., 2004). Reactions (20 µl) contained 30 ng of wildtype plasmid DNA, Q5® High-Fidelity DNA Polymerase (0.4 U), 1x High GC-Enhancer, 1x Q5 Reaction Buffer, 10 mM dNTPs (0.4 µl), and 1 µl each of 10 µM forward and reverse overlapping primers (metabion, Supp. Mat. 1.3). Primers were designed in SnapGene (v6.0.3) with a total length of 50 bp, including 20 bp upstream and 29 bp downstream of the targeted SNV. PCR cycling conditions were 98°C for 30 s; 30 cycles of 98°C for 30 s, 72°C for 45 s and 72°C for 8 min; followed by 72°C for 10 min. For variants located in A/T-rich regions that failed under standard protocol (c.424-151T > G, c.201-14T > G, c.232A > T), conditions were adapted (DeCero et al., 2020). PCR products were treated with DpnI (NEB, R0176L) at 37°C for 1 h to remove methylated parental plasmid DNA and transformed into DH5α cells (NEB, C29871) as described above. Colonies were cultured with ampicillin (100 µg/ml) for 24 hours at 37°C and resistant colonies screened by PCR and Sanger sequencing of the corresponding amplicon (Microsynth).

Cell culture / Transfection

Wildtype and mutant minigenes were transfected separately into HEK293T cells maintained in DMEM/GlutaMAX medium (Gibco, 31966-021) supplemented with 10% FBS (Gibco, 10270106) in a humidified incubator at 37°C and 5% CO_2. Cell cultures were routinely tested for mycoplasma contamination and confirmed to be negative. As the minigene construct did not contain translational start or stop codons or untranslated regions (UTRs), nonsense-mediated decay (NMD) was not expected and therefore not inhibited. Cells were expanded to ~ 90% confluency in T75 flasks (~ 3 x 10^6 cells) and 3.5 × 10^5 cells were seeded into 12-well plates 24 hours before transfection. Transfections were performed using 2.5 µl of Lipofectamine 3000 reagent (Invitrogen, L3000008), 5 µl of P3000 reagent (Invitrogen, L3000008), 100 µl Opti-MEM I (Gibco, 31985062), and 2.5 µg plasmid DNA per well. Twenty-four hours after transfection, cells were transferred to 6-well plates to increase RNA yield, using 1 ml PBS (Sigma-Aldrich, D5652-10X1L) and 0.5 ml trypsin solution (PAN-Biotech, P10-022100) per well. Cells were harvested 48 h post transfection using PBS, and RNAprotect Cell Reagent (Qiagen, 76526), yielding an average of ~ 1.77 × 10^6 cells. RNA was stored at -80°C until further processing.

RNA extraction and targeted RT-PCR

RNA was extracted from HEK293T cells using the RNeasy Mini Kit (Qiagen, 74104), QIAshredder (Qiagen, 79656) and RNase-Free DNase Set (Qiagen, 79256) according to the manufacturer's instructions. RNA yield was quantified using the Qubit RNA BR Assay-Kit (Invitrogen, Q10210). For first strand cDNA synthesis (20 µl reaction volume), 1 µg RNA was mixed with 1 µl Oligo$(dT)_{12-18}$ primer (Invitrogen, 18418012) and 1 µl of 10 mM dNTPs (NEB, N0447S) heated to 65°C for 5 min and immediately chilled on ice. First Strand Buffer (1x, Invitrogen, Y02321), 0.1 M DTT (Invitrogen, PIN Y00147) and 1 µl RNasin Ribonuclease Inhibitor (Promega, N251A) were added. After incubation at 42°C for 2 min, 1 µl SuperScript II (Invitrogen, 18064-022) was incorporated and cDNA synthesis proceeded at 42°C for 1 h, followed by enzyme inactivation at 70°C for 15 min. The resulting cDNA was treated with RNAse H (Qiagen, Y9220L) at 37°C for 20 min and 2 µl were used as template for PCR. PCR reactions (20 µl) contained Q5 High-Fidelity DNA Polymerase (0.2 µl), 1x High GC-Enhancer, 1x Q5 Reaction Buffer, 10 mM dNTPs (0.4 µl), and 1 µl each of 10 µM forward and reverse primers (RT_PCR_plasmid_fwd and RT_PCR_plasmid_rev; Supp. Mat. 1.3). PCR amplification was performed under standardized cycling conditions (98°C for 30 s; 30 cycles of 98°C for 30 s, 65°C for 45 s and 72°C for 2 min; followed by 72°C 10 min), selectively amplifying *SDHB* minigene-derived transcripts (wildtype-amplicon: 931 bp).

Transcriptional analysis

Library preparation and sequencing

Targeted RT-PCR products were prepared for sequencing using the Illumina DNA Prep kit (20018704) according to the manufacturer's protocol. Indexed libraries were sequenced on an Illumina NextSeq 2000 platform generating paired-end 2×150 bp reads, with a minimum depth of 50,000 reads per sample. Raw read quality was assessed with FastQC, and alignment quality metrics were obtained from STAR's Log.final.out and SJ.out.tab files.

Read alignment and splice-junction quantification

Sequencing data were processed using the Spliced Transcripts Alignment to a Reference (STAR) algorithm (Dobin et al., 2013), adapted to a custom minigene reference and optimized parameter settings (GitHub/*SDHB*_minigene/05_NGS_Workflow). Alignment output consisted of BAM files and splice-junction files (SJ.out.tab) for downstream analyses.

Junction detection and splicing annotation

For each variant, all splice junctions contributing > 1% of junctional reads relative to the most abundant wildtype junction were annotated manually with respect to splicing effect (e.g. exon skipping, alternative donor/acceptor usage, cryptic exon inclusion), splice-motif category and supporting read counts. Full intron retentions do not generate splice-junction signals and were therefore manually identified using Integrative Genomics Viewer (IGV v2.12.2) (Robinson et al., 2011). Sashimi plots (Fig. 4) were generated using a modified version of the ggsashimi code, adapted to apply the read-count threshold (> 1% relative proportion) and to display uniquely mapped junction-spanning reads only (GitHub/*SDHB*_minigene/ 08_Additional_Plots_Code).

Transcript reconstruction and quantification

Distinct transcript isoforms were inferred by splice-junction assignments. A junction was considered transcript-specific if it occurred exclusively in a single isoform and was absent from the full-length product and other aberrant isoforms. Transcript proportions were quantified as percent-spliced-in (PSI) (Schafer et al., 2015), adapted to STAR SJ output, by using uniquely mapping reads (Methods Fig. 1, Supp. Mat 1.4). PSI values and inferred transcript structures were aggregated in a curated annotation table (Supp. Table 3).

Methods Fig. 1 *Quantification of transcript ratios by percent-spliced-in (PSI) (*Schafer et al., 2015a). *Schematic illustration of PSI calculation used to quantify relative transcript abundance from targeted RNA sequencing.*

HGVS-based transcript and protein annotation

The effects on transcript and predicted protein level were described using HGVS nomenclature (Hart et al., 2024b). For insertions (intron retention) and deletions (partial or complete exon skipping), an automated procedure was implemented to assign the respective HGVS annotations (GitHub/*SDHB*_minigene/06_Automated_HGVS_Nomenclature). The algorithm reconstructed r.( ) RNA variants from the flanking splice-junction coordinates and inferred the corresponding p.( ) protein consequences by translating the altered mRNA sequence (Baumann, 2021). Complex splicing effects - including pseudo-exons, multi-exon skipping, indels and double intron retentions - were annotated manually (Supp. Mat. 1.5) according to HGVS guidelines, using the UCSC genome browser and the ORF finder tool (Rombel et al., 2002).

Gel-based transcript analysis and Sanger sequencing

In addition to NGS-based quantification of splicing, transcript analysis was performed using agarose gel electrophoresis and Sanger sequencing. RT-PCR products were separated on a 1% agarose gel at 110 V for 75 min and visualized using a Fusion FX Edge imaging system (Vilber). To improve resolution of samples with multiple bands, PCR products were re-run on a 0.8% agarose gel for approximately 2 hours at 110 V. Visible bands were excised from the gel, purified using the QIAquick Gel Extraction Kit (Qiagen, 28704) and re-amplified by nested PCR (RT-PCR primers and conditions) prior to Sanger sequencing. Resulting FASTA files were analyzed using the CLC Workbench (v21.0.3).

RNA Sequencing

Endogenous *SDHB* transcripts of untransfected HEK293T cells were sequenced on the Illumina NextSeq2000 platform following TruSeq Stranded mRNA library prep (Illumina, 20020594) and processed using the alignment and splice-junction analysis described above. Tumor RNA sequencing (Illumina) of MASTER patient 1 and 2 was derived from fresh frozen tumors from the NCT/DKTK/DKFZ MASTER program (Horak et al., 2021; Jahn et al., 2022). Patients consented to banking of tumor and control tissue, molecular profiling of both samples, and clinical data collection (S-206/2011, Ethics Committee of the Medical Faculty of Heidelberg University). The study was conducted in adherence to the Declaration of Helsinki.

Integration of minigene transcriptional data into ACMG workflow

PVS1 was used to capture loss-of-function evidence and BP7 to classify variants without detectable splicing impact, following the recommendations of the ClinGen SVI Splicing Subgroup and (Walker et al., 2023).

We applied a PVS1 strength to each aberrant transcript according to an adapted version (Supp. Figure 2a) of the published PVS1 decision tree (Abou Tayoun et al., 2018) to integrate critical protein regions overlapping with the minigene. We defined the 2Fe-2S ferredoxin-type domain (Pfam Fer2_3), as critical domain (Supp. Figure 2b).

For variants showing both full-length wildtype and aberrant transcripts, we followed the recommended approach of assigning a PVS1 or BP7 strength to each individual transcript, pooling transcripts with the same evidence strength, and then applying an appropriated conservative overall PVS1 (RNA) or BP7 (RNA) strength that considers the relative contribution of each transcript to the overall expression (Walker et al., 2023) (Supp. Figure 2c). Considering the in-vitro setting and published gene specific expert recommendations, e.g. of the ClinGen expert panel for *BRCA1/2* (Parsons et al., 2024), we established cautious thresholds for the overall strength and down-weighted the PVS1 criterion to a maximum strength of strong (Supp. Figure 2d). The BP7 (RNA) code was assigned using a conservative cutoff of ≥ 90% of full-length wildtype transcript (Abou Tayoun et al., 2018; Parsons et al., 2024; Walker et al., 2023). Following evaluation of minigene-derived splicing outcomes, variants were further classified using additional lines of evidence curated in Franklin, a clinical-grade genetic variant interpretation platform (Genoox Ltd., n.d.). ACMG/AMP criteria were applied to variants in accordance with the general guidelines (Richards et al., 2015).

Results

Minigene construction and variant selection

Based on the functionally relevant iron sulfur cluster domains, the exonic reading frame and limitations of plasmid size, we selected exons 2–5 with adjacent intronic sequences as region of interest for a partial *SDHB* minigene. This region was cloned into the mammalian expression vector pcDNA3.1 (Fig. 1a, Supp. Figure 1).

We prioritized splice-associated variants in this region with the *in-silico* prediction tool SpliceAI (Jaganathan et al., 2019), which demonstrated high predictive accuracy and sensitivity (Lord et al., 2025; Smith & Kitzman, 2023). From 340 single nucleotide variants (SNVs) with at least one SpliceAI Δ score above 0.25 (Supp. Table 1), we prioritized 48 variants with a maximum Δ score above 0.42 (range: 0.42–0.97, mean 0.76) for testing (Fig. 1b). SpliceAI predicted acceptor gain for five variants, donor gain for 15 variants, donor-loss for 17 variants, acceptor-loss for one variant and both acceptor and donor loss for 21 variants (all Δ ≥ 0.42) (Fig. 2). Ten variants were located at canonical splice sites (donor or acceptor of exons 3 or 4), 16 were exonic, and 22 were intronic, including three within polypyrimidine tracts. Two additional variants were included as negative controls based on ClinVar and population frequency (gnomAD (Karczewski et al., 2020)), yielding a total of 50 variants. Variant assessment prior to minigene testing yielded two variants as (likely) benign, 14 variants as (likely) pathogenic and 34 variants as variant of uncertain significance. Prioritized variants were introduced in

the vector construct to create 50 minigenes with one SNV each. Wildtype and mutant minigenes were transfected into HEK293T cells and analyzed with a targeted NGS workflow and quantification of splice junctions (relative abundance ≥ 1%) (Fig. 1a).

Transcript analysis of endogenous and minigene derived *SDHB*

Overview of the analyzed genomic regions (intron 2 to intron 4) with annotated splicing elements, including canonical splice sites (orange) and polypyrimidine tracts (yellow). The pre-assessment variant classification prior to integration of RNA evidence was indicated. ((L)P, likely pathogenic/pathogenic; VUS, variant of unknown significance; (L)B, likely benign/benign. Stacked bar plots show the distribution of transcripts assessed by minigene assay for each variant, ratios normalized to 1.0, classified as premature termination codon (PTC, red), full-length (teal), in-frame (yellow), or uncharacterized transcripts (purple). Variants were labeled using HGVS cDNA nomenclature and ordered by genomic position. The lower heatmap displays SpliceAI delta scores (AL, acceptor loss; AG, acceptor gain; DL, donor loss; DG, donor gain), with color intensity indicating predicted splicing impact. (Created with R)

To assess *SDHB* splicing in HEK293T, we performed transcript analysis of endogenous *SDHB*, which revealed a single isoform corresponding to the MANE transcript NM_003000.3 (Supp. Figure 3, Supp. Table 2). Introduction of the wildtype minigene resulted in mRNA corresponding almost completely to the MANE transcript (96%, NM_003000.3). Only very low fractions of exon 3 skipping (out of frame, 2%) and partial exon 4 skipping (out of frame, 2%) were observed (Fig. 2, Supp. Table 3). In addition, substantially low levels (< 1%) of a 54-nucleotide in-frame partial exon 4 skipping were detected, corresponding to the *SDHB* isoform ENST00000485515.6. This isoform is ubiquitously expressed at very low levels across tissues (typically < 1 TPM) according to GTEx data (GTEx Consortium, 2020). Based on these findings, endogenous *SDHB* in HEK293T and *SDHB* minigene derived transcript profile closely resembled splicing of biologically relevant *SDHB* transcripts, supporting its suitability for investigating the transcriptional impact of *in-silico* predicted splice-associated variants.

While 14 out of 50 variants (28.0%), including two negative controls, showed solely wildtype transcript, at least one aberrant transcript was detected for 36 variants (72.0%) (Fig. 2). The average number of observed transcripts per variant was 2.3 (median two, range one to six), including 40 full-length wildtype-transcripts and 73 aberrant transcripts, resulting in a total of 113 transcripts (Supp. Table 3). Observed aberrant splicing among 73 transcripts included partial exon skipping (42.5%, n = 31 transcripts from 18 variants), single exon skipping (26%, n = 19 transcripts from 19 variants), intron retention (13.7%, 10 transcripts from 10 variants), pseudo-exon inclusion (11%, 8 transcripts from 6 variants), and multi-exon skipping (6.8%, 5 transcripts from 5 variants) (Supp. Figures 4 and 5). While 20% of aberrant transcripts (n = 14 of 73 transcripts from 13 variants) preserved the reading frame, 80% of aberrant transcripts (n = 59 of 73 from 35 variants) led to an expected premature termination codon (PTC) (Fig. 2, Supp. Table 3). Among the 34 variants leading to ≥ 2 aberrant transcripts, 26 were found to express both aberrantly spliced transcript(s) and wildtype-transcript. Three aberrant transcripts could not be fully characterized, as they represented whole intron retention events within the minigene at low relative abundance (< 5%). As the minigene construct contains only limited flanking intronic sequence, these events could not be reliably evaluated in the endogenous genomic context. Among 48 variants prioritized by SpliceAI (Δ ≥ 0.42), 17 (35%) exhibited ≥ 90% aberrant splicing, confirming splice disruption. In contrast, 19 variants (40%) with a SpliceAI Δ score ≥ 0.42 showed ≥ 90% wildtype expression, indicating preserved splicing despite high *in-silico* splice disruption scores (Fig. 2). An additional five variants located near the minigene boundaries were tested, but splicing outcomes could not be reliably assessed due to the absence of adjacent splice sites within the construct (Supp. Table 3, “no functional assessment”).

The comparison of targeted NGS-based transcript analysis with conventional gel electrophoresis followed by Sanger sequencing of visible and excised bands revealed a clear advantage of the NGS-approach. Only 47% of transcripts (53 of 113) identified by NGS could be detected by gel electrophoresis and Sanger sequencing, particularly failing to capture small splicing alterations and unexpected effects (Supp. Figure 6a and 6b). In addition, this alternative approach did not allow reliable transcript identification and quantification (Supp. Figure 6, 7, 8).

Taken together, the *SDHB* minigene assay proved suitable for splicing analysis and enabled experimental confirmation of aberrant splicing for nearly three quarters of *in-silico* prioritized variants.

Integration of RNA analysis into ACMG/AMP variant classification

Table 1

Integration of variant-specific splicing outcomes into ACMG/AMP classification for SDHB variants.

Variant selection			Transcript analysis			ACMG classification			
Variant (HGVSc)	**HGVSp (pre-assesment)**	**Class (pre-asesment)**	**PVS1_Strength**	**BP7_S**	**Combined strength**	**Overall RNA strength**	**ACMG codes with RNA strength**	**ACMG points with RNA strength**	**ACMG class with RNA strength**
c.201-14T > G	p.?	VUS	PVS1: 0.74 (r.201_286del, p.(Cys68HisfsTer21)); 0.09 (r.200_201ins[201 – 13_201-1], p.(Lys67AsnfsTer4))	0.17 (FL_WT)	PVS1 (0.83) + BP7_S (0.17)	PVS1_Moderate (RNA)	PM2 Supporting PVS1 Moderate (RNA)	3	VUS
c.201-1G > C	p.?	P	PVS1: 0.40 (r.201_202del, p.(Cys68TrpfsTer11)); 0.36 (r.201_234del, p.(Cys68LeufsTer8)); 0.09 (r.200_201ins[201-4_201-1], p.(Lys67AsnfsTer14)); 0.08 (r.201_286del, p.(Cys68HisfsTer21)) PVS1_M: 0.05 (r.201_206del, p.(Lys67_Gly69del))	0.03 (FL_WT)	PVS1 (0.93) + PVS1_M (0.05) + BP7_S (0.03)	PVS1_Strong (RNA)	PVS1 Strong (RNA) PS1 Strong PM2 Supporting	9	LP
c.201-2A > C	p.?	P	PVS1: 0.89 (r.201_286del, p.(Cys68HisfsTer21)); 0.06 (r.201_234del, p.(Cys68LeufsTer8)); 0.02 (r.200_201ins[201-4_201-1], p.(Lys67AsnfsTer14))	0.03 (FL_WT)	PVS1 (0.97) + BP7_S (0.03)	PVS1_Strong (RNA)	PVS1 Strong (RNA) PS1 Strong PM2 Supporting PS4 Moderate	11	P
c.201-2A > T	p.?	P	PVS1: 0.89 (r.201_286del, p.(Cys68HisfsTer21)); 0.07 (r.201_234del, p.(Cys68LeufsTer8))	0.04 (FL_WT)	PVS1 (0.96) + BP7_S (0.04)	PVS1_Strong (RNA)	PVS1 Strong (RNA) PS1 Strong PM2 Supporting	9	LP
c.201-3T > A	p.?	VUS	PVS1: 0.34 (r.201_286del, p.(Cys68HisfsTer21))	0.66 (FL_WT)	PVS1 (0.34) + BP7_S (0.66)	PVS1_N/A (RNA)[6]	not applicable[6]	N/A	N/A
c.201-91C > G	p.?	VUS	PVS1: 0.27 (r.200-201ins[201–211_201 – 92], p.(Cys68AsnTer6)); 0.03 (r.200-201ins[201–226_201 – 92], p.(Lys67AsnTer12))	0.65 (FL_WT)	PVS1 (0.30) + BP7_S (0.65) + N/A (0.05)[1]	PVS1_N/A (RNA)[6]	not applicable[6]	N/A	N/A
c.201-96A > G	p.?	VUS	PVS1: 0.35 (r.200-201ins[201–211_201 – 97], p.(Cys68AsnTer6)); 0.04 (r.200-201ins[201–226_201 – 97], p.(Lys67AsnTer12))	0.61 (FL_WT)	PVS1 (0.39) + BP7_S (0.61)	PVS1_N/A (RNA)[6]	not applicable[6]	N/A	N/A
c.202T > A	p.Cys68Ser	VUS	PVS1: 0.11 (r.201_286del, p.(Cys68HisfsTer21)) PVS1_M: 0.02 (r.201_203del, p.(Lys67_Cys68del))	0.87 (FL_WT)	PVS1 (0.11) + PVS1_M (0.02) + BP7_S (0.87)	PVS1_N/A (RNA)[6]	not applicable[6]	N/A	N/A

Variant selection			Transcript analysis			ACMG classification			
Variant (HGVSc)	**HGVSp (pre-assesment)**	**Class (pre-asesment)**	**PVS1_Strength**	**BP7_S**	**Combined strength**	**Overall RNA strength**	**ACMG codes with RNA strength**	**ACMG points with RNA strength**	**ACMG class with RNA strength**
c.219G > A	p.Leu73=	VUS	-	1.00 (FL_WT)	BP7_S (1.00)	BP7_S (RNA)	PM2 Supporting PP3 Supporting BP7 Strong (RNA)	-2	LB
c.225T > C	p.Ala75=	LB	-	1.00 (FL_WT)	BP7_S (1.00)	BP7_S (RNA)	PM2 Supporting BS2 Supporting BP7 Strong (RNA)	-4	LB
c.232A > T	p.Lys78Ter	LP	PVS1: 0.06 (r.201_286del, p.(Cys68HisfsTer21))	0.94 (FL_WT)	PVS1 (0.06) + BP7_S (0.94)	BP7_S (RNA) not applicable[7]	not applicable[7]	N/A	N/A
c.245A > T	p.Glu82Val	VUS	-	1.00 (FL_WT)	BP7_S (1.00)	BP7_S (RNA) not applicable[7]	not applicable[7]	N/A	N/A
c.286 + 1G > A	p.?	P	PVS1: 0.75 (r.286_287ins[286 + 1_286 + 144], p.(Gly96AspfsTer37)); 0.25 (r.201_286del, p.(Cys68HisfsTer21))	-	PVS1 (1.00)	PVS1_Strong (RNA)	PVS1 Strong (RNA) PS1 Strong PM2 Supporting PS4 Moderate	11	P
c.286 + 2T > A	p.?	P	PVS1: 0.50 (r.201_286del, p.(Cys68HisfsTer21)); 0.50 (r.286_287ins[286 + 1_286 + 144], p.(Ile97GlufsTer36))	-	PVS1 (1.00)	PVS1_Strong (RNA)	PVS1 Strong (RNA) PS1 Strong PM2 Supporting PS4 Moderate	11	P
c.286 + 3G > C	p.?	VUS	PVS1: 0.64 (r.201_286del, p.(Cys68HisfsTer21)); 0.04 (r.286_287ins[286 + 1_286 + 144], p.(Ile97GlnfsTer36))	0.32 (FL_WT)	PVS1 (0.68) + BP7_S (0.32)	PVS1_N/A (RNA)[6]	not applicable[6]	N/A	N/A
c.286 + 4A > T	p.?	VUS	PVS1: 0.42 (r.201_286del, p.(Cys68HisfsTer21)); 0.07 (r.286_287ins[286 + 1_286 + 144], p.(Ile97ValfsTer36))	0.51 (FL_WT)	PVS1 (0.49) + BP7_S (0.51)	PVS1_N/A (RNA)[6]	not applicable[6]	N/A	N/A
c.286 + 5G > C	p.?	VUS	PVS1: 0.30 (r.201_286del, p.(Cys68HisfsTer21)); 0.13 (r.286_287ins[286 + 1_286 + 144], p.(Ile97AspfsTer36))	0.57 (FL_WT)	PVS1 (0.43) + BP7_S (0.57)	PVS1_N/A (RNA)[6]	not applicable[6]	N/A	N/A

Variant selection			Transcript analysis			ACMG classification			
Variant (HGVSc)	**HGVSp (pre-assesment)**	**Class (pre-asesment)**	**PVS1_Strength**	**BP7_S**	**Combined strength**	**Overall RNA strength**	**ACMG codes with RNA strength**	**ACMG points with RNA strength**	**ACMG class with RNA strength**
c.286G > C	p.Gly96Arg	VUS	PVS1: 0.30 (r.201_286del, p.(Cys68HisfsTer21)); 0.19 (r.286_287ins[286 + 1_286 + 144], p.(Gly96ArgfsTer37))	0.51 (FL_WT)	PVS1 (0.49) + BP7_S (0.51)	PVS1_N/A (RNA)[6]	not applicable[6]	N/A	N/A
c.287-10T > G	p.?	VUS	-	1.00 (FL_WT)	BP7_S (1.00)	BP7_S (RNA)	PM2 Supporting PP3 Supporting BP7 Strong (RNA)	-2	LB
c.287-12T > A	p.?	VUS	-	1.00 (FL_WT)	BP7_S (1.00)	BP7_S (RNA)	PM2 Supporting PP3 Supporting BP7 Strong (RNA)	-2	LB
c.287-1G > C	p.?	P	PVS1: 0.86 (r.287_423del, p.(Ile97PhefsTer11)); 0.04 (r.201_423del, p.(Cys68IleTer2)); 0.03 (r.287_411del, p.(Ile97SerfsTer15)) PVS1_S: 0.04 (r.287_322del, p.(Ile97_Gly108del))	-	PVS1 (0.93) + PVS1_S (0.04) + N/A (0.03)[2]	PVS1_Strong (RNA)	PVS1 Strong (RNA) PS1 Strong PM2 Supporting PS4 Moderate	11	P
c.287-1G > T	p.?	P	PVS1: 0.64 (r.287_423del, p.(Ile97PhefsTer11)); 0.07 (r.287_411del, p.(Ile97SerfsTer15)); 0.04 (r.201_423del, p.(Cys68IleTer2)) PVS1_S: 0.18 (r.287_322del, p.(Ile97_Gly108del)); 0.03 (r.287_334del, p.(Gly96_Leu111del))	0.01 (FL_WT)	PVS1 (0.75) + PVS1_S (0.21) + BP7_S (0.01) + N/A (0.04)[2]	PVS1_Strong (RNA)[3]	PVS1 Strong (RNA) PS1 Strong PM2 Supporting	9	LP
c.287-2A > T	p.?	P	PVS1: 0.98 (r.287_423del, p.(Ile97PhefsTer11)); 0.02 (r.201_423del, p.(Cys68IleTer2))	-	PVS1 (1.00)	PVS1_Strong (RNA)	PVS1 Strong (RNA) PS1 Strong PM2 Supporting	9	LP
c.287-3C > G	p.?	LP	PVS1: 0.82 (r.287_423del, p.(Ile97PhefsTer11)); 0.03 (r.201_423del, p.(Cys68IleTer2)); 0.01 (r.287_411del, p.(Ile97SerfsTer15))	0.14 (FL_WT)	PVS1 (0.86) + BP7_S (0.14)	PVS1_Moderate (RNA)	PM2 Supporting PS4 Moderate PVS1 Moderate (RNA) PS1 Moderate	7	LP
c.287-5T > G	p.?	VUS	PVS1: 0.04 (r.287_423del, p.	0.94 (FL_WT)	PVS1 (0.06) +	BP7_S (RNA)	PM2 Supporting	-2	LB

Variant selection			Transcript analysis			ACMG classification			
Variant (HGVSc)	**HGVSp (pre-assesment)**	**Class (pre-asesment)**	**PVS1_Strength**	**BP7_S**	**Combined strength**	**Overall RNA strength**	**ACMG codes with RNA strength**	**ACMG points with RNA strength**	**ACMG class with RNA strength**
			(Ile97PhefsTer11)); 0.02 (r.201_423del, p.(Cys68IleTer2))		BP7_S (0.94)		PP3 Supporting BP7 Strong (RNA)		
c.287-6T > G	p.?	VUS	PVS1: 0.02 (r.287_423del, p.(Ile97PhefsTer11))	0.98 (FL_WT)	PVS1 (0.02) + BP7_S (0.98)	BP7_S (RNA)	PM2 Supporting PP3 Supporting BP7 Strong (RNA)	-2	LB
c.287-8T > G	p.?	VUS	-	1.00 (FL_WT)	BP7_S (1.00)	BP7_S (RNA)	PM2 Supporting PP3 Supporting BP7 Strong (RNA)	-2	LB
c.287G > T	p.Gly96Val	VUS	-	1.00 (FL_WT)	BP7_S (1.00)	BP7_S (RNA) not applicable[7]	not applicable[7]	N/A	N/A
c.300T > C	p.Ser100=	B	-	1.00 (FL_WT)	BP7_S (1.00)	BP7_S (RNA)	BS1 Strong BS2 Strong BP7 Strong (RNA)	-12	B
c.365A > G	p.Asn122Ser	VUS	-	1.00 (FL_WT)	BP7_S (1.00)	BP7_S (RNA) not applicable[7]	not applicable[7]	N/A	N/A
c.372C > A	p.Val124=	VUS	PVS1_N/A: 0.97 (r.370_423del5, p.(Val124_Pro141del))[5]	0.03 (FL_WT)	BP7_S (0.03) + PVS1_N/A (0.97)[5]	PVS1_N/A[5]	not applicable[5]	N/A	N/A
c.398T > G	p.Met133Arg	VUS	PVS1: 1.00 (r.399_423del, p.(Met133ArgfsTer2))	-	PVS1 (1.00)	PVS1_Strong (RNA)	PM2 Supporting PVS1 Strong (RNA)	5	VUS
c.399G > C	p.Met133Ile	VUS	-	1.00 (FL_WT)	BP7_S (1.00)	BP7_S (RNA) not applicable[7]	not applicable[7]	N/A	N/A
c.400T > G	p.Tyr134Asp	VUS	-	1.00 (FL_WT)	BP7_S (1.00)	BP7_S (RNA) not applicable[7]	not applicable[7]	N/A	N/A
c.401A > T	p.Tyr134Phe	VUS	-	1.00 (FL_WT)	BP7_S (1.00)	BP7_S (RNA) not applicable[7]	not applicable[7]	N/A	N/A
c.402T > A	p.Tyr134Ter	LP	PVS1: 1.00 (r.399_423del, p.(Tyr134IlefsTer1))	-	PVS1 (1.00)	PVS1_Strong (RNA)	PVS1 Strong (RNA) PM2 Supporting	5	VUS
c.403G > T	p.Val135Leu	VUS	-	1.00 (FL_WT)	BP7_S (1.00)	BP7_S (RNA) not applicable[7]	not applicable[7]	N/A	N/A
c.413A > G	p.Asp138Gly	VUS	PVS1: 0.15 (r.399_423del, p.(Tyr134IlefsTer1))	0.68 (FL_WT)	PVS1 (0.15) + BP7_S (0.68) +	PVS1_N/A[5]	not applicable[5]	N/A	N/A

Variant selection			Transcript analysis			ACMG classification			
Variant (HGVSc)	**HGVSp (pre-assesment)**	**Class (pre-asesment)**	**PVS1_Strength**	**BP7_S**	**Combined strength**	**Overall RNA strength**	**ACMG codes with RNA strength**	**ACMG points with RNA strength**	**ACMG class with RNA strength**
			PVS1_N/A: 0.17 (r.370_423del5, p.(Val124_Pro141del))[5]		PVS1_N/A (0.17)[5]				
c.423 + 156G > T	p.?	VUS	PVS1: 0.11 (r.423_424ins[423 + 161_423 + 288], p.(Asp142GluTer35))	0.89 (FL_WT)	PVS1 (0.11) + BP7_S (0.89)	BP7_S (RNA)[4]	PM2 Supporting PP3 Supporting BP7 Strong (RNA)	-2	LB
c.423 + 190A > C	p.?	VUS	PVS1: 0.01 (r.423_424ins[423 + 161_423 + 288], p.(Asp142GluTer35))	0.99 (FL_WT)	PVS1 (0.01) + BP7_S (0.99)	BP7_S (RNA)	PM2 Supporting PP3 Supporting BP7 Strong (RNA)	-2	LB
c.423 + 1G > T	p.?	P	PVS1: 0.73 (r.399_423del, p.(Tyr134IlefsTer1)) PVS1_N/A: 0.27 (r.370_423del5, p.(Val124_Pro141del))[5]	-	PVS1 (0.73) + PVS1_N/A (0.27)[5]	PVS1_N/A[5]	not applicable[5]	N/A	N/A
c.423 + 294G > T	p.?	VUS	PVS1: 0.09 (r.423_424ins[423 + 161_423 + 288], p.(Asp142GluTer35))	0.91 (FL_WT)	PVS1 (0.09) + BP7_S (0.91)	BP7_S (RNA)	PM2 Supporting PP3 Supporting BP7 Strong (RNA)	-2	LB
c.423 + 296T > A	p.?	VUS	PVS1: 0.03 (r.423_424ins[423 + 161_423 + 293], p.(Asp142GluTer35))	0.97 (FL_WT)	PVS1 (0.03) + BP7_S (0.97)	BP7_S (RNA)	PM2 Supporting PP3 Supporting BP7 Strong (RNA)	-2	LB
c.423 + 2T > G	p.?	P	PVS1: 0.49 (r.399_423del, p.(Tyr134IlefsTer1)) PVS1_N/A: 0.51 (r.370_423del5, p.(Val124_Pro141del))[5]	-	PVS1 (0.49) + PVS1_N/A (0.51)[5]	PVS1_N/A[5]	not applicable[5]	N/A	N/A
c.423 + 3G > T	p.?	VUS	PVS1: 0.63 (r.399_423del, p.(Tyr134IlefsTer1)) PVS1_N/A: 0.35 (r.370_423del5, p.(Val124_Pro141del))[5]	0.02 (FL_WT)	PVS1 (0.63) + BP7_S (0.02) + PVS1_N/A (0.35)[5]	PVS1_N/A[5]	not applicable[5]	N/A	N/A
c.423 + 4A > T	p.?	VUS	PVS1: 0.69 (r.399_423del, p.(Tyr134IlefsTer1)) PVS1_N/A: 0.31 (r.370_423del5, p.(Val124_Pro141del))[5]	-	PVS1 (0.69) + PVS1_N/A (0.31)[5]	PVS1_N/A[5]	not applicable[5]	N/A	N/A
c.423 + 5G > C	p.?	LP	PVS1: 0.72 (r.399_423del, p.(Tyr134IlefsTer1))	-	PVS1 (0.72) +	PVS1_N/A[5]	not applicable[5]	N/A	N/A

Variant selection			Transcript analysis			ACMG classification			
Variant (HGVSc)	**HGVSp (pre-assesment)**	**Class (pre-asesment)**	**PVS1_Strength**	**BP7_S**	**Combined strength**	**Overall RNA strength**	**ACMG codes with RNA strength**	**ACMG points with RNA strength**	**ACMG class with RNA strength**
			PVS1_N/A: 0.28 (r.370_423del5, p.(Val124_Pro141del))[5]		PVS1_N/A (0.28)[5]				
c.423 + 6T > G	p.?	VUS	PVS1: 0.46 (r.399_423del, p.(Tyr134IlefsTer1)) PVS1_N/A: 0.53 (r.370_423del5, p.(Val124_Pro141del))[5]	0.02 (FL_WT)	PVS1 (0.46) + BP7_S (0.02) + PVS1_N/A (0.53)[5]	PVS1_N/A[5]	not applicable[5]	N/A	N/A
c.423C > G	p.Pro141=	VUS	-	1.00 (FL_WT)	BP7_S (1.00)	BP7_S (RNA)	PM2 Supporting PP3 Supporting BP7 Strong (RNA)	-2	LB
c.424-151T > G	p.?	VUS	PVS1: 0.03 (r.399_423del, p.(Tyr134IlefsTer1)); 0.02 (r.423_424ins[424 – 150_424-1], p.(Asp142IlefsTer18)) PVS1_N/A: 0.04 (r.370_423del5, p.(Val124_Pro141del))[5]	0.91 (FL_WT)	PVS1 (0.05) + BP7_S (0.91) + PVS1_N/A (0.04)[5]	BP7_S (RNA)	PM2 Supporting PP3 Supporting BP7 Strong (RNA)	-2	LB

Overview of all tested *SDHB* variants (n = 50) with identified transcripts and fractions, HGVS nomenclature and ACMG classifications for variants with conclusive transcript data with and without minigene derived RNA code. An extended version of this table, including ACMG evidence codes and point assignments prior to RNA evidence integration, is provided in Supplementary Table 4. **Footnotes**: [1]Total intron 2 retention (r.200_201ins[200 + 1_201-1], p.(Cys68Ter)). [2]Total intron 3 retention (r.286_287ins[286 + 1_287-1], p.(Ile97GlufsTer36)). [3]PVS1_Strong (RNA) overall strength assigned due to overall high percentage of splice disruption. [4]BP7_S ratio rounded up. [5]Transcript corresponds to the alternative *SDHB* isoform ENST00000485515.6; overall RNA strength was not assigned if abundance was ≥ 10%. [6]Overall RNA strength was not assigned because transcript(s) did not meet predefined interpretation thresholds. [7]No aberrant splicing was observed in the splicing assay; however, BP7 was not applied due potential missense effect. FL_WT, full-length wildtype transcript; PVS1_S, strong PVS1 strength; PVS1_M, moderate PVS1 strength; PVS1_N/A, PVS1 not assigned; BP7_S, strong BP7 strength; (L)P, (likely) pathogenic; VUS, variant of unknown significance; (L)B, (likely) benign.

To integrate gained transcriptional insights into a criterion for variant classification according to Tayoun and Walker (Abou Tayoun et al., 2018; Walker et al., 2023), we adapted the PVS1 decision tree to the gene and assay to assign weighted PVS1 at the transcript level (Supp. Figure 2a). All aberrant transcripts leading to a premature termination codon (PTC) and thereby predicted to result in loss of function (LoF) received a PVS1_Strong code. In-frame transcripts predicted to disrupt functionally critical regions were likewise assigned a PVS1_Strong code (Supp. Figure 2a and 2b). We applied BP7_Strong to full-length wildtype transcripts. Accordingly, a PVS1/BP7_strength code was assigned to 104 transcripts (Supp. Table 3, Table 1) and yielded 59 times PVS1 (52.2%), three times PVS1_Strong (2.7%), twice PVS1_Moderate (1.8%) and 40 times BP7_Strong (35.4%). PVS1_Strong was given to three in-frame transcripts leading to partial deletions within the functionally critical 2Fe-2S ferredoxin-type domain (Pfam Fer2_3). PVS1_Moderate was assigned to two variants that led to small in-frame deletions within the Fer2_3 domain (Supp. Figure 2b). Nine transcripts could not be assigned a strength code (PVS1_N/A), as all corresponded to an in-frame 54-nt partial exon 4 skipping (r.370_423del) matching the lowly expressed transcript ENST00000485515.6 detected across multiple normal tissues (GTEx Consortium, 2020) (Supp. Figure 2b).

In addition, we developed a complementary decision tree to combine PVS1 and BP7 evidence, allowing assignment of an overall weighted PVS1 and BP7 (RNA) strength based on the observed transcriptional impact and relative transcript fraction (Supp. Figure 2c). An overall PVS1_strength (RNA) or BP7_Strong (RNA) was assigned per variant, with PVS1_strength code proportionally downweighed to a conservative maximum of strong (Supp. Figure 2d). For variants with multiple transcripts, individual transcript-level codes were combined using conservative thresholds (≥ 80% loss-of-function transcripts for PVS1_strength (RNA) (BRCA1/2 VCEP guidelines (Parsons et al., 2024)), ≥ 90% wildtype transcript for BP7_Strong (RNA)) to derive an overall RNA strength (Supp. Figure 2c, Table 1). This approach yielded a total of PVS1_Strong (RNA) codes for 10 variants (including eight canonical splice-site variants), PVS1_Moderate (RNA) codes for two variants, and BP7_Strong (RNA) codes for 14 intronic or synonymous variants (Table 1). For the eight missense variants with a SpliceAI Δ ≥ 0.42 but ≥ 90% wildtype-transcript, we did not apply BP7_strong (RNA), as a deleterious coding impact of the missense variant could not be ruled out. In addition, eight variants with complex splicing effects did not reach the predefined thresholds for an

overall RNA strength. Moreover, eight variants (including two canonical splice-site variants) yielding ≥ 10% of the alternative splice product r.370_423del (ENST00000485515.6) were not assigned an overall RNA strength as a conservative measure given the uncertain protein impact of this transcript.

To assess the added value of minigene-derived RNA analyses and PVS1/BP7 (RNA) code evidence, we compared the point-based and total five-class ACMG/AMP assessment with and without RNA data for 26 variants that received an RNA code (Fig. 3, Supp. Table 4). Incorporation of RNA evidence resulted in an average ACMG point change (Δ) of 2.7 points (median Δ = 3.5 points; range: 1–4), with an increase for three variants (11.5%) and a decrease for 23 variants (88.5%) (Fig. 3). A class-switch based on minigene data was identified for 17 variants (65.4%), resulting in a clinically meaningful reclassification for 13 variants (50%): 12 (of 13, 92.3%) were reclassified from VUS to likely benign, and one variant (c.402T > A, of 13, 7.7%) from likely pathogenic to VUS.

Selected variants and comparison of minigene to primary cancer data

We observed distinct aberrant and alternative splicing patterns for selected variants (Fig. 4a). Aberrant splicing was identified for two coding variants located in exon 4 (Fig. 4a, top). Both the missense variant c.398T > G (p.Met133Arg) and, interestingly, the stop-gain variant c.402T > A (p.Tyr134Ter), induced partial exon 4 skipping (r.399_423del, including the variant position c.402T > A) and resulted in a frameshift transcripts with a novel premature stop codon (p.(Met133ArgfsTer2) for c.398T > G and p.(Tyr134IlefsTer1) for c.402T > A). These findings revealed a splicing-based mechanism of pathogenicity, rather than the anticipated missense or direct truncating effect.

In addition to coding and splice-site variants, two intronic variants located outside canonical splice junctions exhibited pronounced splice disruption in the minigene assay (Fig. 4a, bottom). The intronic variant c.201-14T > G in the polypyrimidine tract resulted in extensive aberrant splicing, with more than 80% of transcripts harboring a premature termination codon due to exon 3 skipping (74%, r.201_286del, p.(Cys68HisfsTer21)) or a 13-nt intron 3 retention (9%, r.200_201ins[201 − 13_201-1], p.(Lys67AsnfsTer4)). The intronic variant c.287-3C > G predominantly induced exon 4 skipping (r.287_423del, p.(Ile97PhefsTer11)), accounting for 82% of all detected transcripts, with two additional low-abundance splice alterations including skipping of two exons (3 and 4, 3%) and a 125-nt partial exon 4 skipping (1%). Overall, 86% of aberrant transcripts were predicted to lead to premature termination codons. Furthermore, we detected the in-frame 54-nt partial exon 4 skipping event (r.370_423del, p.(Val124_Pro141del), which was also observed in the wildtype minigene and normal tissues at very low levels (< 1%), for eight variants with an abundance ≥ 10% (Table 1, Supp. Table 3). Notably, the synonymous variant c.372C > A (p.Val124=) almost exclusively produced this isoform (97%). Similarly, two canonical splice-site variants (c.423 + 2T > G and c.423 + 1G > T) yielded this alternative transcript at substantial levels (51% and 27%), in addition to a frameshifting transcript (r.399_423del, p.(Tyr134IlefsTer1)) with 49% and 73% relative proportion.

To further confirm the validity of our minigene assay, we compared minigene results to splicing in primary human cancers and identified two variants as germline alterations in two participants of the precision oncology study NCT/DKTK/DKFZ MASTER (Horak et al., 2021; Jahn et al., 2022) (Fig. 4b). Within this program, DNA sequencing of fresh frozen tumor and blood as well as RNA sequencing of fresh frozen tumor tissue is performed. For the exon 3 canonical donor variant c.286 + 1G > A (Fig. 4b, top), germline heterozygosity was confirmed in blood DNA (variant allele frequency (VAF) 48%). Tumor DNA sequencing from a gastrointestinal stromal tumor (GIST) demonstrated near-complete loss of the wildtype allele (VAF 93%), consistent with loss of heterozygosity (LoH) as a likely second hit. Tumor RNA sequencing (tumor cell content 89%) revealed exon 3 skipping and activation of a cryptic donor site within intron 3, resulting in a 144-nt intron 3 retention (r.286_287ins[286 + 1_286 + 144]). A heterozygous germline coding variant within this patient in exon 4 also showed loss of heterozygosity in tumor DNA (VAF in blood 56%, tumor 96%). However, in tumor RNA the exonic variant was only partially present (VAF ~ 39%), which likely indicated nonsense mediated decay of the allele with the pathogenic germline variant and wildtype transcript of the normal tissue. In line with these observations, the minigene assay reproduced both splice events, demonstrating 75% intron 3 retention and 25% exon 3 skipping.

In a second patient with the heterozygous exon 4 canonical acceptor variant c.287-1G > C (VAF 55%), we interrogated DNA and RNA from a metastatic endometrial stromal sarcoma (Fig. 4b, bottom). Tumor DNA showed an unchanged VAF (53%) and no evidence of a second hit at the *SDHB* locus. RNA sequencing (tumor cell content 87%) revealed exon 4 skipping (r.287_423del, p.(Ile97PhefsTer11)) with very low splice junction read count. Notably, another germline variant in exon 1 demonstrated preserved heterozygosity in tumor DNA (VAF in blood 42%, tumor 51%) but near-complete monoallelic expression in tumor RNA (VAF 100%), indicating extensive allele-specific transcript degradation by nonsense-mediated decay. In line with this observation, the minigene assay revealed predominant exon 4 skipping (86%), and additional low-level splice isoforms predicted to introduce PTCs (exon 3 and exon 4 skipping, partial exon 4 skipping) for this variant. Together, these observations support the validity of the minigene assay and showcase its suitability to quantify transcripts leading to PTC, which cannot be routinely performed for tumor tissue with expected biologically relevant expression.

Discussion

We established a minigene encompassing a critical region of *SDHB* spanning exons 2–5, enabling systematic assessment of 48 splice-associated variants prioritized by SpliceAI. Targeted NGS-based cDNA sequencing revealed substantial transcript diversity, with 113 variant-associated minigene transcripts detected across all tested variants. Aberrant splicing exceeding 10% of the total transcript abundance was observed for almost half of the investigated variants of uncertain significance (16 of 34). Integration of these transcriptional findings into an RNA-based ACMG/AMP evidence framework resulted in assignment of RNA codes to approximately half of the variants, underscoring both the sensitivity of transcript-level assays and the challenges of translating complex splicing patterns into robust variant-level conclusions.

SpliceAI (Jaganathan et al., 2019) is a benchmarked (Rowlands et al., 2021) and widely used *in silico* tool to explore potential splice-altering effects. While high SpliceAI scores are generally associated with splice disruption, our data indicate that intermediate prediction scores - particularly for non-canonical intronic and exonic variants - frequently correspond to predominantly wildtype splicing, underscoring the limited specificity of *in-silico* prioritization and the need for transcript-based functional validation, especially for deep intronic variants (Jaganathan et al., 2019). Novel in-silico prediction tools or their combination might be beneficial (Kurosawa et al., 2023; Wagner et al., 2023).

Comparison of targeted NGS-based transcript profiling with conventional gel electrophoresis followed by Sanger sequencing (Dong et al., 2023; Nix et al., 2022) revealed that approximately half of the transcript isoforms detected by NGS would likely have escaped detection by conventional methods. While this precludes direct comparison with fragment analysis commonly used in minigene assays (Acedo et al., 2015; Bueno-Martínez et al., 2022; Sanoguera-Miralles et al., 2024), it highlights the substantially increased sensitivity of NGS-based approaches to resolve complex splice events. These findings align with recent methodological advances emphasizing the complexity of transcript structures generated in minigene assays and the need for refined analytical strategies, including dedicated isoform reconstruction tools (Aucouturier et al., 2025) and long-read sequencing approaches that enable full-length transcript resolution and phasing (Pardo-Palacios et al., 2024).

While targeted transcript analysis was highly sensitive for detecting low-abundance transcripts, translating transcript effects into robust evidence strengths proved challenging. Although transcript-level PVS1/BP7_strength assignments were possible for ≥ 90% of detected transcripts, only a subset of variants (≈ 50%) met conservative cut-offs for combined-strength aggregation. Reasons were potential impact of missense variants on protein level, transcript fractions below predefined thresholds, or the presence of alternative splicing patterns. The incorporation of transcript-level data into an ACMG/AMP framework resulted in shifts of ACMG points (Tavtigian et al., 2018) for 54% of all tested variants, predominantly reflecting a reduction in inferred pathogenicity. However, these shifts did not consistently translate into clinically actionable classification changes, underscoring that transcript-based evidence is best interpreted as a complementary evidence layer integrated with additional functional, clinical, and population-based information. In line with a conservative interpretation of minigene data, the *BRCA1/2* guidelines (Parsons et al., 2024) recommend a maximum evidence weight of strong for functional splicing assays. Notably, for Lynch syndrome-associated genes, minigene-based validation of aberrant splicing observed in constitutional normal tissues is recommended (Spier et al., 2024). Consistent with the limitations observed in our dataset, large-scale functional studies using saturation genome editing (SGE) have demonstrated that functional scores can resolve the majority of variants across clinically relevant genes such as *BRCA2, BAP1, DDX3X* and *VHL* (Buckley et al., 2024; Huang et al., 2025; Radford et al., 2023; Sahu et al., 2025; Waters et al., 2024), but a non-negligible fraction remains intermediate or unresolved, emphasizing that no single assay can fully adjudicate all variants (Huang et al., 2025; Radford et al., 2023).

In line with this, alternative splicing events illustrated the complexity of variant interpretation. An in-frame transcript isoform (r.370_423del, p.(Val124_Pro141del) (ENST00000485515.6), was detected at low levels in the wildtype minigene but increased over 10% abundance in eight variants. As the protein-level impact of this isoform remains undefined, these variants could not be assigned an RNA-based ACMG criteria. Structural annotation (UniProt, PDB) suggested that resulting 18-aa-deletion affects the Fer2_3 domain and may alter interaction interfaces (chain A/C) and β-sheet architecture. Notably, the alternative 54-bp in-frame skipping event has been experimentally demonstrated *in vivo* for the splice-donor variant c.423 + 1G > A by RT-PCR analysis of patient-derived tumor RNA from two individuals with PPGL (Bayley et al., 2006). A distinct splice-donor variant at the same position, c.423 + 1G > T, has likewise been identified in a PPGL patient (Li et al., 2023). Consistent with these observations, our minigene assay showed that c.423 + 1G > T generated the identical in-frame skipping at a relative proportion of 27%, supporting the clinical relevance of this isoform while highlighting the need for protein-level functional validation. Recently, a protein-level functional assay for *SDHB* variants has been reported, which could provide complementary insights beyond transcript-based readouts, especially for missense variants without impact on splicing (Lee et al., 2025). Aberrant splicing was also observed for the missense variant c.398T > G (p.Met133Arg) and the stop-gain variant c.402T > A (p.Tyr134Ter), emphasizing that splice-altering effects are not restricted to canonical splice-site changes but can occur across variant classes. Sensitive transcript-based assays are therefore essential to detect variant-specific splice outcomes and may provide a functional framework for evaluating splice-modulating strategies, including splice-switching antisense oligonucleotides, engineered snRNA-based approaches, and small-molecule splicing modifiers (Fernandez Alanis et al., 2012; Havens & Hastings, 2016; Naryshkin et al., 2014). Together, these observations highlight that integrative interpretation across multiple functional layers will be required to fully resolve the molecular and clinical consequences of splice-associated variants, possibly enabling therapeutic approaches.

Although genome-editing approaches provide complementary advantages by interrogating variants within their native genomic context and enabling transcriptome-wide readouts (Buckley et al., 2024; Findlay et al., 2018), they introduce additional experimental and analytical complexity, including confounding effects of gDNA abundance, NMD and cellular fitness. For deep intronic variants, genome-editing strategies based on homology-directed repair (HDR) face additional technical constrains, whereas emerging base- and prime-editing approaches may expand the scope of functional interrogation (Belli et al., 2025; Herger et al., 2025). In contrast, minigenes assays offer a splicing-focused and interpretable readout that allows direct variant attribution and quantification of observed effects, making them particularly well suited for experimental validation of splice-associated predictions, despite limitations related to their artificial genomic context and reduced tissue-specific regulation (Buisine et al., 2025). Recently developed barcoded minigene approaches further enable pooled, NGS-based assessment of splicing events at increased throughput (O'Neill et al., 2024) although such strategies remain constrained by assay design and transcript detection.

A shared limitation of genome-editing and minigene assays is the potential divergence of tissue-specific splicing from biologically relevant effects. However, endogenous RNA sequencing of HEK293T cells revealed predominant expression of the *SDHB* MANE transcript (NM_003000.3), consistent with low alternative splicing across GTEx tissues. Additionally, a substantial overlap between minigene-derived and tumor-derived splice products was

observed for selected variants. Nevertheless, evaluation of selected variants in iPSC-based models (e.g., chromaffin cells, sympathetic neurons, neural-crest–derived cells) could further approximate native, tissue-specific splice regulation. Interpretation of patient-derived RNA sequencing remains challenging, particularly in the context of nonsense-mediated decay and loss of heterozygosity, which can obscure allele-specific splice effects and distort quantitative inference from steady-state RNA. Consistent with this limitation, tumor RNA sequencing confirmed variant-consistent aberrant splicing but did not permit reliable quantification of variant-induced effects. Tumor RNA interpretation could be improved by phasing through long-read sequencing. In contrast, the minigene assay enabled direct, allele-independent measurement of splice outcomes, providing a complementary and mechanistically interpretable functional readout.

Conclusions

By implementing an *SDHB* exon 2–5 minigene model in HEK293T cells, we provided a validated framework for the systematic assessment of splice-associated variants. Integration of targeted NGS, semi-automated HGVS annotation, and ACMG/AMP-based curation framework enables a scalable strategy for assessing splice-associated variants of unknown significance and thereby narrowing the diagnostic gap in *SDHB*-related diseases. Our findings emphasize that accurate variant interpretation requires identification of precise molecular consequences rather than reliance on generic loss-of-function assumptions, with relevance for both germline and somatic variant assessment and future therapeutic considerations. We expect that multiplexed minigene-based approaches, combined with genome-editing and complementary functional assays, will advance characterization of splice-associated variants. Such strategies hold promises for dissecting context- and tissue-dependent effects of *SDHB* biology and for informing integrative models of variant interpretation and precision medicine.

Supplementary Files

Figures

Supplemental_Figures.pdf

Supplemental Fig. 1 Schematic representation of *SDHB* minigene with exons 2 to 5

Supplemental Fig. 2 ACMG/AMP decision trees

Supplemental Fig. 3 Sashimi plot of RNA-Seq data of endogenous *SDHB* in HEK293T

Supplemental Fig. 4 Bar chart showing distribution of splice effects

Supplemental Fig. 5 Bar chart showing observed splice effects per ACMG/AMP code

Supplemental Fig. 6 Results from Gel-electrophoresis of RT-PCR products

Supplemental Fig. 7 Bar chart transcripts identified by NGS vs Sanger/Gel

Supplemental Fig. 8 Bar chart showing difference in resolution of transcript number comparing NGS approach with conventional Gel/sanger method

Tables

Supp_Tab_1_SpliceAI_prioritization.xlsx Supp_Tab_2_Splice_junction_analysis.xlsx

Supp_Tab_3_Transcript_analysis_results.xlsx Supp_Tab_4_Extented_Tab_1.xlsx

Material

Supplemental_Material.pdf

Declarations

Data availability

All related code for the *SDHB* minigene project as well as minigene reference is available from GitHub (https://github.com/AnniKoehler/*SDHB*_minigene/tree/main). BAM- and splice-junction files will be deposited at the German Human Genome Archive (GHGA). Variants and minigene readout will be uploaded to the ClinVar database.

Acknowledgements

A.K. was supported by the Mildred Scheel Doctoral Program of the German Cancer Aid andnon-financially supported by the Carus Promotionskolleg (CPKD) of the Medical Faculty of the Technical University Dresden. This work was supported (non-financially) by the European Reference Network on

Genetic Tumor Risk Syndromes (ERN GENTURIS) - Project ID No 739547. ERN GENTURIS is partly co-funded by the European Union within the framework of the Third Health Program ERN-2016 — Framework Partnership Agreement 2017-2021.

Author Contributions

Concept and design: A.K., A.A.B., A.C.G, A.J. Drafting of the manuscript: A.K., N.L., A.J. Bioinformatics: A.A.B., A.K., D.W., Administrative, technical, or material support: A.R., D.W., D.L.D, E.S. Supervision: E.S., A.J. All the authors contributed for critical revision of the manuscript for important intellectual content, acquisition, analysis, or interpretation of data, accountability for all aspects of the work in ensuring that questions related to the accuracy or integrity of any part of the work are appropriately investigated and resolved and final approval of completed version of manuscript.

Funding

This study was funded by the NCT Dresden and the Mildred Scheel Doctoral Program of the German Cancer Aid. The MASTER program is supported by the NCT Overarching Clinical Translational Trial Program, the NCT Heidelberg Molecular Precision Oncology Program, and DKTK.

Conflicts of Interest

S.F.: Honoraria: Illumina. E.S.: Honoraria: Illumina. A.J.: Honoraria: AstraZeneca. The other authors declare no competing interests.

References

1. Abou Tayoun, A. N., Pesaran, T., DiStefano, M. T., Oza, A., Rehm, H. L., Biesecker, L. G., Harrison, S. M., & ClinGen Sequence Variant Interpretation Working Group (ClinGen SVI). (2018). Recommendations for interpreting the loss of function PVS1 ACMG/AMP variant criterion. *Human Mutation*, *39*(11), 1517–1524. https://doi.org/10.1002/humu.23626
2. Acedo, A., Hernández-Moro, C., Curiel-García, Á., Díez-Gómez, B., & Velasco, E. A. (2015). Functional classification of BRCA2 DNA variants by splicing assays in a large minigene with 9 exons. *Human Mutation*, *36*(2), 210–221. https://doi.org/10.1002/humu.22725
3. Amar, L., Bertherat, J., Baudin, E., Ajzenberg, C., Bressac-de Paillerets, B., Chabre, O., Chamontin, B., Delemer, B., Giraud, S., Murat, A., Niccoli-Sire, P., Richard, S., Rohmer, V., Sadoul, J.-L., Strompf, L., Schlumberger, M., Bertagna, X., Plouin, P.-F., Jeunemaitre, X., & Gimenez-Roqueplo, A.-P. (2005). Genetic testing in pheochromocytoma or functional paraganglioma. *Journal of Clinical Oncology: Official Journal of the American Society of Clinical Oncology*, *23*(34), 8812–8818. https://doi.org/10.1200/JCO.2005.03.1484
4. Aucouturier, C., Goardon, N., Castéra, L., Atkinson, A., Lavolé, T., Legros, A., Ricou, A., Boulouard, F., Krieger, S., & Leman, R. (2025). Decipher RNA isoform combinations from minigene splicing assays and massive parallel sequencing with MAGIC. *Bioinformatics (Oxford, England)*, *41*(9), btaf525. https://doi.org/10.1093/bioinformatics/btaf525
5. Baumann, A. A. (2021). *Characterization of putative splice site mutations in cancer-predisposition associated genes by integration of genome and transcriptome data*.
6. Bayley, J.-P., van Minderhout, I., Weiss, M. M., Jansen, J. C., Oomen, P. H., Menko, F. H., Pasini, B., Ferrando, B., Wong, N., Alpert, L. C., Williams, R., Blair, E., Devilee, P., & Taschner, P. E. (2006). Mutation analysis of *SDHB* and SDHC: Novel germline mutations in sporadic head and neck paraganglioma and familial paraganglioma and/or pheochromocytoma. *BMC Medical Genetics*, *7*, 1. https://doi.org/10.1186/1471-2350-7-1
7. Belli, O., Karava, K., Farouni, R., & Platt, R. J. (2025). Multimodal scanning of genetic variants with base and prime editing. *Nature Biotechnology*, *43*(9), 1458–1470. https://doi.org/10.1038/s41587-024-02439-1
8. Buckley, M., Terwagne, C., Ganner, A., Cubitt, L., Brewer, R., Kim, D.-K., Kajba, C. M., Forrester, N., Dace, P., De Jonghe, J., Shepherd, S. T. C., Sawyer, C., McEwen, M., Diederichs, S., Neumann-Haefelin, E., Turajlic, S., Ivakine, E. A., & Findlay, G. M. (2024). Saturation genome editing maps the functional spectrum of pathogenic VHL alleles. *Nature Genetics*, *56*(7), 1446–1455. https://doi.org/10.1038/s41588-024-01800-z
9. Bueno-Martínez, E., Sanoguera-Miralles, L., Valenzuela-Palomo, A., Esteban-Sánchez, A., Lorca, V., Llinares-Burguet, I., Allen, J., García-Álvarez, A., Pérez-Segura, P., Durán, M., Easton, D. F., Devilee, P., Vreeswijk, M. P., De La Hoya, M., & Velasco-Sampedro, E. A. (2022). Minigene-based splicing analysis and ACMG / AMP -based tentative classification of 56 *ATM* variants. *The Journal of Pathology*, *258*(1), 83–101. https://doi.org/10.1002/path.5979
10. Buisine, M.-P., Bellanne-Chantelot, C., Calmels, N., Vaché, C., Besnard, T., Cogne, B., Vitobello, A., Piton, A., Martins, A., Gaildrat, P., Dhaenens, C.-M., Gorokhova, S., Boutry-Kryza, N., Caputo, S., Leman, R., Krieger, S., Le Gac, G., & Houdayer, C. (2025). RNA-based diagnostic studies in genetics: Review and guidance from a multidisciplinary French network. *European Journal of Human Genetics*, *33*(10), 1219–1227. https://doi.org/10.1038/s41431-025-01881-2
11. Burnichon, N., Rohmer, V., Amar, L., Herman, P., Leboulleux, S., Darrouzet, V., Niccoli, P., Gaillard, D., Chabrier, G., Chabolle, F., Coupier, I., Thieblot, P., Lecomte, P., Bertherat, J., Wion-Barbot, N., Murat, A., Venisse, A., Plouin, P.-F., Jeunemaitre, X., … PGL.NET network. (2009). The succinate dehydrogenase genetic testing in a large prospective series of patients with paragangliomas. *The Journal of Clinical Endocrinology and Metabolism*, *94*(8), 2817–2827. https://doi.org/10.1210/jc.2008-2504

12. Canson, D. M., Llinares-Burguet, I., Fortuno, C., Sanoguera-Miralles, L., Bueno-Martínez, E., de la Hoya, M., Spurdle, A. B., & Velasco-Sampedro, E. A. (2025). TP53 minigene analysis of 161 sequence changes provides evidence for role of spatial constraint and regulatory elements on variant-induced splicing impact. *NPJ Genomic Medicine*, *10*(1), 37. https://doi.org/10.1038/s41525-025-00498-0
13. DeCero, S. A., Winslow, C. H., & Coburn, J. (2020). Method to Overcome Inefficiencies in Site-Directed Mutagenesis of A/T-Rich DNA. *Journal of Biomolecular Techniques: JBT*, *31*(3), 94–99. https://doi.org/10.7171/jbt.20-3103-003
14. Dobin, A., Davis, C. A., Schlesinger, F., Drenkow, J., Zaleski, C., Jha, S., Batut, P., Chaisson, M., & Gingeras, T. R. (2013). STAR: Ultrafast universal RNA-seq aligner. *Bioinformatics (Oxford, England)*, *29*(1), 15–21. https://doi.org/10.1093/bioinformatics/bts635
15. Dong, Z., Wang, Y., Zhang, J., Zhu, F., Liu, Z., Kang, Y., Lin, M., & Shi, H. (2023). Analyzing the effects of BRCA1/2 variants on mRNA splicing by minigene assay. *Journal of Human Genetics*, *68*(2), 65–71. https://doi.org/10.1038/s10038-022-01077-2
16. Fassnacht, M., Dekkers, O., Else, T., Baudin, E., Berruti, A., de Krijger, R., Haak, H., Mihai, R., Assie, G., & Terzolo, M. (2018). European Society of Endocrinology Clinical Practice Guidelines on the management of adrenocortical carcinoma in adults, in collaboration with the European Network for the Study of Adrenal Tumors. *European Journal of Endocrinology*, *179*(4), G1–G46. https://doi.org/10.1530/EJE-18-0608
17. Fernandez Alanis, E., Pinotti, M., Dal Mas, A., Balestra, D., Cavallari, N., Rogalska, M. E., Bernardi, F., & Pagani, F. (2012). An exon-specific U1 small nuclear RNA (snRNA) strategy to correct splicing defects. *Human Molecular Genetics*, *21*(11), 2389–2398. https://doi.org/10.1093/hmg/dds045
18. Findlay, G. M., Daza, R. M., Martin, B., Zhang, M. D., Leith, A. P., Gasperini, M., Janizek, J. D., Huang, X., Starita, L. M., & Shendure, J. (2018). Accurate classification of BRCA1 variants with saturation genome editing. *Nature*, *562*(7726), 217–222. https://doi.org/10.1038/s41586-018-0461-z
19. Fraile-Bethencourt, E., Valenzuela-Palomo, A., Díez-Gómez, B., Caloca, M. J., Gómez-Barrero, S., & Velasco, E. A. (2019). Minigene Splicing Assays Identify 12 Spliceogenic Variants of BRCA2 Exons 14 and 15. *Frontiers in Genetics*, *10*, 503. https://doi.org/10.3389/fgene.2019.00503
20. Genoox Ltd. (n.d.). *Franklin by Genoox* (Version v85.3) [Computer software]. Retrieved October 1, 2025, from https://franklin.genoox.com
21. GTEx Consortium. (2020). The GTEx Consortium atlas of genetic regulatory effects across human tissues. *Science (New York, N.Y.)*, *369*(6509), 1318–1330. https://doi.org/10.1126/science.aaz1776
22. Hart, R. K., Fokkema, I. F. A. C., DiStefano, M., Hastings, R., Laros, J. F. J., Taylor, R., Wagner, A. H., & den Dunnen, J. T. (2024a). HGVS Nomenclature 2024: Improvements to community engagement, usability, and computability. *Genome Medicine*, *16*(1), 149. https://doi.org/10.1186/s13073-024-01421-5
23. Hart, R. K., Fokkema, I. F. A. C., DiStefano, M., Hastings, R., Laros, J. F. J., Taylor, R., Wagner, A. H., & den Dunnen, J. T. (2024b). HGVS Nomenclature 2024: Improvements to community engagement, usability, and computability. *Genome Medicine*, *16*(1), 149. https://doi.org/10.1186/s13073-024-01421-5
24. Havens, M. A., & Hastings, M. L. (2016). Splice-switching antisense oligonucleotides as therapeutic drugs. *Nucleic Acids Research*, *44*(14), 6549–6563. https://doi.org/10.1093/nar/gkw533
25. Herger, M., Kajba, C. M., Buckley, M., Cunha, A., Strom, M., & Findlay, G. M. (2025). High-throughput screening of human genetic variants by pooled prime editing. *Cell Genomics*, *5*(4), 100814. https://doi.org/10.1016/j.xgen.2025.100814
26. Horak, P., Heining, C., Kreutzfeldt, S., Hutter, B., Mock, A., Hüllein, J., Fröhlich, M., Uhrig, S., Jahn, A., Rump, A., Gieldon, L., Möhrmann, L., Hanf, D., Teleanu, V., Heilig, C. E., Lipka, D. B., Allgäuer, M., Ruhnke, L., Laßmann, A., … Fröhling, S. (2021). Comprehensive Genomic and Transcriptomic Analysis for Guiding Therapeutic Decisions in Patients with Rare Cancers. *Cancer Discovery*, *11*(11), 2780–2795. https://doi.org/10.1158/2159-8290.CD-21-0126
27. Huang, H., Hu, C., Na, J., Hart, S. N., Gnanaolivu, R. D., Abozaid, M., Rao, T., Tecleab, Y. A., CARRIERS Consortium, Pesaran, T., Lyra, P. C. M., Karam, R., Yadav, S., Nathanson, K. L., Domchek, S. M., de la Hoya, M., Robson, M., Mehine, M., Bandlamudi, C., … Couch, F. J. (2025). Functional evaluation and clinical classification of BRCA2 variants. *Nature*, *638*(8050), 528–537. https://doi.org/10.1038/s41586-024-08388-8
28. Jaganathan, K., Panagiotopoulou, S. K., McRae, J. F., Darbandi, S. F., Knowles, D., Li, Y. I., Kosmicki, J. A., Arbelaez, J., Cui, W., Schwartz, G. B., Chow, E. D., Kanterakis, E., Gao, H., Kia, A., Batzoglou, S., Sanders, S. J., & Farh, K. K.-H. (2019). Predicting Splicing from Primary Sequence with Deep Learning. *Cell*, *176*(3), 535–548.e24. https://doi.org/10.1016/j.cell.2018.12.015
29. Jahn, A., Rump, A., Widmann, T. J., Heining, C., Horak, P., Hutter, B., Paramasivam, N., Uhrig, S., Gieldon, L., Drukewitz, S., Kübler, A., Bermudez, M., Hackmann, K., Porrmann, J., Wagner, J., Arlt, M., Franke, M., Fischer, J., Kowalzyk, Z., … Klink, B. (2022). Comprehensive cancer predisposition testing within the prospective MASTER trial identifies hereditary cancer patients and supports treatment decisions for rare cancers. *Annals of Oncology: Official Journal of the European Society for Medical Oncology*, *33*(11), 1186–1199. https://doi.org/10.1016/j.annonc.2022.07.008
30. Karczewski, K. J., Francioli, L. C., Tiao, G., Cummings, B. B., Alföldi, J., Wang, Q., Collins, R. L., Laricchia, K. M., Ganna, A., Birnbaum, D. P., Gauthier, L. D., Brand, H., Solomonson, M., Watts, N. A., Rhodes, D., Singer-Berk, M., England, E. M., Seaby, E. G., Kosmicki, J. A., … MacArthur, D. G. (2020). The mutational constraint spectrum quantified from variation in 141,456 humans. *Nature*, *581*(7809), 434–443. https://doi.org/10.1038/s41586-020-2308-7
31. Kurosawa, R., Iida, K., Ajiro, M., Awaya, T., Yamada, M., Kosaki, K., & Hagiwara, M. (2023). PDIVAS: Pathogenicity predictor for Deep-Intronic Variants causing Aberrant Splicing. *BMC Genomics*, *24*(1), 601. https://doi.org/10.1186/s12864-023-09645-2
32. Landrum, M. J., Lee, J. M., Riley, G. R., Jang, W., Rubinstein, W. S., Church, D. M., & Maglott, D. R. (2014). ClinVar: Public archive of relationships among sequence variation and human phenotype. *Nucleic Acids Research*, *42*(Database issue), D980-985. https://doi.org/10.1093/nar/gkt1113
33. Lee, S., Needleman, L., Park, J., Schugar, R., Guo, Q., Ford, J., & Annes, J. (2025). Functional Characterization of *SDHB* Variants Clarifies Hereditary Pheochromocytoma and Paraganglioma Risk and Genotype–Phenotype Relationships. *Journal of Clinical Investigation*.

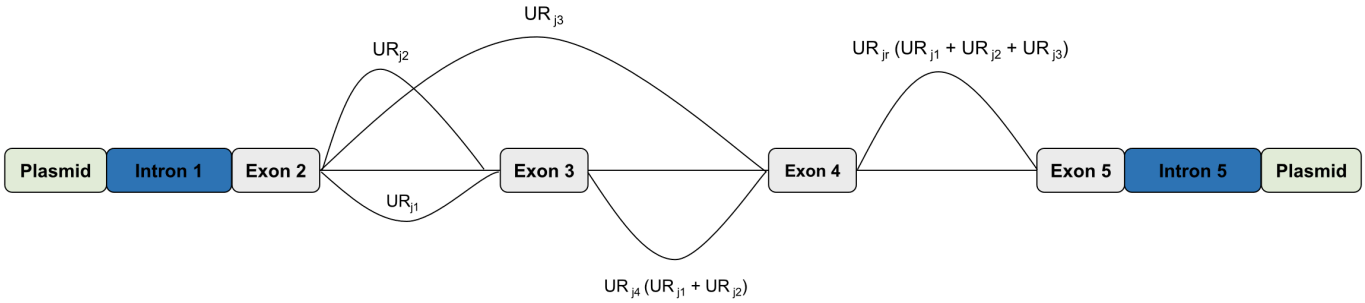
https://doi.org/10.1172/JCI198165

34. Li, C., Li, J., Han, C., Wang, T., Zhang, L., Wang, Z., Wang, T., Xu, L., Qi, G., Qin, G., Li, X., & Zheng, L. (2023). Novel and recurrent genetic variants of VHL, *SDHB*, and RET genes in Chinese pheochromocytoma and paraganglioma patients. *Frontiers in Genetics*, *14*, 959989. https://doi.org/10.3389/fgene.2023.959989
35. Lord, J., Oquendo, C. J., Wai, H. A., Douglas, A. G. L., Bunyan, D. J., Wang, Y., Hu, Z., Zeng, Z., Danis, D., Katsonis, P., Williams, A., Lichtarge, O., Chang, Y., Bagnall, R. D., Mount, S. M., Matthiasardottir, B., Lin, C., Hansen, T. van O., Leman, R., … Baralle, D. (2025). Predicting the impact of rare variants on RNA splicing in CAGI6. *Human Genetics*, *144*(2–3), 243–251. https://doi.org/10.1007/s00439-023-02624-3
36. Morales, J., Pujar, S., Loveland, J. E., Astashyn, A., Bennett, R., Berry, A., Cox, E., Davidson, C., Ermolaeva, O., Farrell, C. M., Fatima, R., Gil, L., Goldfarb, T., Gonzalez, J. M., Haddad, D., Hardy, M., Hunt, T., Jackson, J., Joardar, V. S., … Murphy, T. D. (2022). A joint NCBI and EMBL-EBI transcript set for clinical genomics and research. *Nature*, *604*(7905), 310–315. https://doi.org/10.1038/s41586-022-04558-8
37. Naryshkin, N. A., Weetall, M., Dakka, A., Narasimhan, J., Zhao, X., Feng, Z., Ling, K. K. Y., Karp, G. M., Qi, H., Woll, M. G., Chen, G., Zhang, N., Gabbeta, V., Vazirani, P., Bhattacharyya, A., Furia, B., Risher, N., Sheedy, J., Kong, R., … Metzger, F. (2014). Motor neuron disease. SMN2 splicing modifiers improve motor function and longevity in mice with spinal muscular atrophy. *Science (New York, N.Y.)*, *345*(6197), 688–693. https://doi.org/10.1126/science.1250127
38. Nix, P., Mundt, E., Coffee, B., Goossen, E., Warf, B. M., Brown, K., Bowles, K., & Roa, B. (2022). Interpretation of BRCA2 Splicing Variants: A Case Series of Challenging Variant Interpretations and the Importance of Functional RNA Analysis. *Familial Cancer*, *21*(1), 7–19. https://doi.org/10.1007/s10689-020-00224-y
39. O'Neill, M. J., Yang, T., Laudeman, J., Calandranis, M. E., Harvey, M. L., Solus, J. F., Roden, D. M., & Glazer, A. M. (2024). ParSE-seq: A calibrated multiplexed assay to facilitate the clinical classification of putative splice-altering variants. *Nature Communications*, *15*(1), 8320. https://doi.org/10.1038/s41467-024-52474-4
40. Pardo-Palacios, F. J., Wang, D., Reese, F., Diekhans, M., Carbonell-Sala, S., Williams, B., Loveland, J. E., De María, M., Adams, M. S., Balderrama-Gutierrez, G., Behera, A. K., Gonzalez Martinez, J. M., Hunt, T., Lagarde, J., Liang, C. E., Li, H., Meade, M. J., Moraga Amador, D. A., Prjibelski, A. D., … Brooks, A. N. (2024). Systematic assessment of long-read RNA-seq methods for transcript identification and quantification. *Nature Methods*, *21*(7), 1349–1363. https://doi.org/10.1038/s41592-024-02298-3
41. Parsons, M. T., de la Hoya, M., Richardson, M. E., Tudini, E., Anderson, M., Berkofsky-Fessler, W., Caputo, S. M., Chan, R. C., Cline, M. S., Feng, B.-J., Fortuno, C., Gomez-Garcia, E., Hadler, J., Hiraki, S., Holdren, M., Houdayer, C., Hruska, K., James, P., Karam, R., … Spurdle, A. B. (2024). Evidence-based recommendations for gene-specific ACMG/AMP variant classification from the ClinGen ENIGMA BRCA1 and BRCA2 Variant Curation Expert Panel. *American Journal of Human Genetics*, *111*(9), 2044–2058. https://doi.org/10.1016/j.ajhg.2024.07.013
42. Radford, E. J., Tan, H.-K., Andersson, M. H. L., Stephenson, J. D., Gardner, E. J., Ironfield, H., Waters, A. J., Gitterman, D., Lindsay, S., Abascal, F., Martincorena, I., Kolesnik-Taylor, A., Ng-Cordell, E., Firth, H. V., Baker, K., Perry, J. R. B., Adams, D. J., Gerety, S. S., & Hurles, M. E. (2023). Saturation genome editing of DDX3X clarifies pathogenicity of germline and somatic variation. *Nature Communications*, *14*(1), 7702. https://doi.org/10.1038/s41467-023-43041-4
43. Rehm, H. L., Berg, J. S., Brooks, L. D., Bustamante, C. D., Evans, J. P., Landrum, M. J., Ledbetter, D. H., Maglott, D. R., Martin, C. L., Nussbaum, R. L., Plon, S. E., Ramos, E. M., Sherry, S. T., & Watson, M. S. (2015). ClinGen—The Clinical Genome Resource. *New England Journal of Medicine*, *372*(23), 2235–2242. https://doi.org/10.1056/NEJMsr1406261
44. Richards, S., Aziz, N., Bale, S., Bick, D., Das, S., Gastier-Foster, J., Grody, W. W., Hegde, M., Lyon, E., Spector, E., Voelkerding, K., Rehm, H. L., & ACMG Laboratory Quality Assurance Committee. (2015). Standards and guidelines for the interpretation of sequence variants: A joint consensus recommendation of the American College of Medical Genetics and Genomics and the Association for Molecular Pathology. *Genetics in Medicine: Official Journal of the American College of Medical Genetics*, *17*(5), 405–424. https://doi.org/10.1038/gim.2015.30
45. Robinson, J. T., Thorvaldsdóttir, H., Winckler, W., Guttman, M., Lander, E. S., Getz, G., & Mesirov, J. P. (2011). Integrative Genomics Viewer. *Nature Biotechnology*, *29*(1), 24–26. https://doi.org/10.1038/nbt.1754
46. Rombel, I. T., Sykes, K. F., Rayner, S., & Johnston, S. A. (2002). ORF-FINDER: A vector for high-throughput gene identification. *Gene*, *282*(1–2), 33–41. https://doi.org/10.1016/s0378-1119(01)00819-8
47. Rowlands, C., Thomas, H. B., Lord, J., Wai, H. A., Arno, G., Beaman, G., Sergouniotis, P., Gomes-Silva, B., Campbell, C., Gossan, N., Hardcastle, C., Webb, K., O'Callaghan, C., Hirst, R. A., Ramsden, S., Jones, E., Clayton-Smith, J., Webster, A. R., Douglas, A. G. L., … Ellingford, J. M. (2021). Comparison of in silico strategies to prioritize rare genomic variants impacting RNA splicing for the diagnosis of genomic disorders. *Scientific Reports*, *11*(1), 20607. https://doi.org/10.1038/s41598-021-99747-2
48. Sahu, S., Galloux, M., Southon, E., Caylor, D., Sullivan, T., Arnaudi, M., Zanti, M., Geh, J., Chari, R., Michailidou, K., Papaleo, E., & Sharan, S. K. (2025). Saturation genome editing-based clinical classification of BRCA2 variants. *Nature*, *638*(8050), 538–545. https://doi.org/10.1038/s41586-024-08349-1
49. Sanoguera-Miralles, L., Bueno-Martínez, E., Valenzuela-Palomo, A., Esteban-Sánchez, A., Llinares-Burguet, I., Pérez-Segura, P., García-Álvarez, A., De La Hoya, M., & Velasco-Sampedro, E. A. (2022). Minigene Splicing Assays Identify 20 Spliceogenic Variants of the Breast/Ovarian Cancer Susceptibility Gene RAD51C. *Cancers*, *14*(12), 2960. https://doi.org/10.3390/cancers14122960
50. Sanoguera-Miralles, L., Valenzuela-Palomo, A., Bueno-Martínez, E., Esteban-Sánchez, A., Lorca, V., Llinares-Burguet, I., García-Álvarez, A., Pérez-Segura, P., Infante, M., Easton, D. F., Devilee, P., Vreeswijk, M. P. G., De La Hoya, M., & Velasco-Sampedro, E. A. (2024). Systematic Minigene-Based

Splicing Analysis and Tentative Clinical Classification of 52 *CHEK2* Splice-Site Variants. *Clinical Chemistry*, *70*(1), 319–338. https://doi.org/10.1093/clinchem/hvad125

51. Schafer, S., Miao, K., Benson, C. C., Heinig, M., Cook, S. A., & Hubner, N. (2015). Alternative Splicing Signatures in RNA-seq Data: Percent Spliced in (PSI). *Current Protocols in Human Genetics*, *87*, 11.16.1-11.16.14. https://doi.org/10.1002/0471142905.hg1116s87
52. *SDHB gene – Gene ID: 6390*. (n.d.). National Center for Biotechnology Information (NCBI). Retrieved October 1, 2024, from https://www.ncbi.nlm.nih.gov/gene/6390
53. Smith, C., & Kitzman, J. O. (2023). Benchmarking splice variant prediction algorithms using massively parallel splicing assays. *Genome Biology*, *24*(1), 294. https://doi.org/10.1186/s13059-023-03144-z
54. Spier, I., Yin, X., Richardson, M., Pineda, M., Laner, A., Ritter, D., Boyle, J., Mur, P., Hansen, T. V. O., Shi, X., Mahmood, K., Plazzer, J.-P., Ognedal, E., Nordling, M., Farrington, S. M., Yamamoto, G., Baert-Desurmont, S., Martins, A., Borras, E., … InSiGHT-ClinGen Hereditary Colon Cancer/Polyposis Variant Curation Expert Panel. (2024). Gene-specific ACMG/AMP classification criteria for germline APC variants: Recommendations from the ClinGen InSiGHT Hereditary Colorectal Cancer/Polyposis Variant Curation Expert Panel. *Genetics in Medicine: Official Journal of the American College of Medical Genetics*, *26*(2), 100992. https://doi.org/10.1016/j.gim.2023.100992
55. Tavtigian, S. V., Greenblatt, M. S., Harrison, S. M., Nussbaum, R. L., Prabhu, S. A., Boucher, K. M., Biesecker, L. G., & ClinGen Sequence Variant Interpretation Working Group (ClinGen SVI). (2018). Modeling the ACMG/AMP variant classification guidelines as a Bayesian classification framework. *Genetics in Medicine: Official Journal of the American College of Medical Genetics*, *20*(9), 1054–1060. https://doi.org/10.1038/gim.2017.210
56. The UniProt Consortium. (n.d.). *UniProt entry P21912 – SDHB* [Dataset]. Retrieved October 1, 2024, from https://www.uniprot.org/uniprotkb/P21912/entry
57. van der Klift, H. M., Jansen, A. M. L., van der Steenstraten, N., Bik, E. C., Tops, C. M. J., Devilee, P., & Wijnen, J. T. (2015). Splicing analysis for exonic and intronic mismatch repair gene variants associated with Lynch syndrome confirms high concordance between minigene assays and patient RNA analyses. *Molecular Genetics & Genomic Medicine*, *3*(4), 327–345. https://doi.org/10.1002/mgg3.145
58. Wagner, N., Çelik, M. H., Hölzlwimmer, F. R., Mertes, C., Prokisch, H., Yépez, V. A., & Gagneur, J. (2023). Aberrant splicing prediction across human tissues. *Nature Genetics*, *55*(5), 861–870. https://doi.org/10.1038/s41588-023-01373-3
59. Walker, L. C., Hoya, M. de la, Wiggins, G. A. R., Lindy, A., Vincent, L. M., Parsons, M. T., Canson, D. M., Bis-Brewer, D., Cass, A., Tchourbanov, A., Zimmermann, H., Byrne, A. B., Pesaran, T., Karam, R., Harrison, S. M., Spurdle, A. B., & ClinGen Sequence Variant Interpretation Working Group. (2023). Using the ACMG/AMP framework to capture evidence related to predicted and observed impact on splicing: Recommendations from the ClinGen SVI Splicing Subgroup. *American Journal of Human Genetics*, *110*(7), 1046–1067. https://doi.org/10.1016/j.ajhg.2023.06.002
60. Waters, A. J., Brendler-Spaeth, T., Smith, D., Offord, V., Tan, H. K., Zhao, Y., Obolenski, S., Nielsen, M., van Doorn, R., Murphy, J.-E., Gupta, P., Rowlands, C. F., Hanson, H., Delage, E., Thomas, M., Radford, E. J., Gerety, S. S., Turnbull, C., Perry, J. R. B., … Adams, D. J. (2024). Saturation genome editing of BAP1 functionally classifies somatic and germline variants. *Nature Genetics*, *56*(7), 1434–1445. https://doi.org/10.1038/s41588-024-01799-3
61. Zheng, L., Baumann, U., & Reymond, J.-L. (2004). An efficient one-step site-directed and site-saturation mutagenesis protocol. *Nucleic Acids Research*, *32*(14), e115. https://doi.org/10.1093/nar/gnh110

Figures



$$TR_{j_x} = \frac{UR_{j_x}}{UR_{j_r}}$$

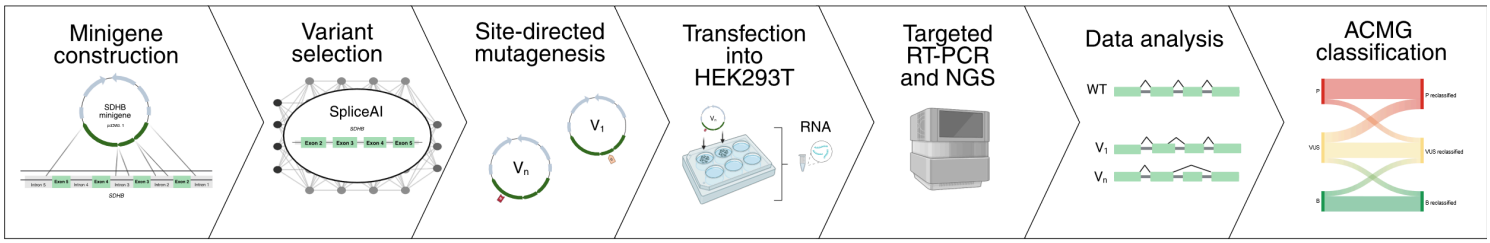
$$RN_{j_x} = \frac{UR_{j_x}}{\sum_{n=1}^{i} UR_{jn}}$$

UR	uniquely mapping reads crossing a splice junction
TR	transcript ratio
RN	normalized transcript ratio
j_x	transcript *(x)* defining splice junction
j_r	reference splice junction
i	total number of splice junctions defining the transcripts

Figure 1

Methods Figure 1 Quantification of transcript ratios by percent-spliced-in (PSI) (Schafer et al., 2015a). Schematic illustration of PSI calculation used to quantify relative transcript abundance from targeted RNA sequencing.

a)



b)

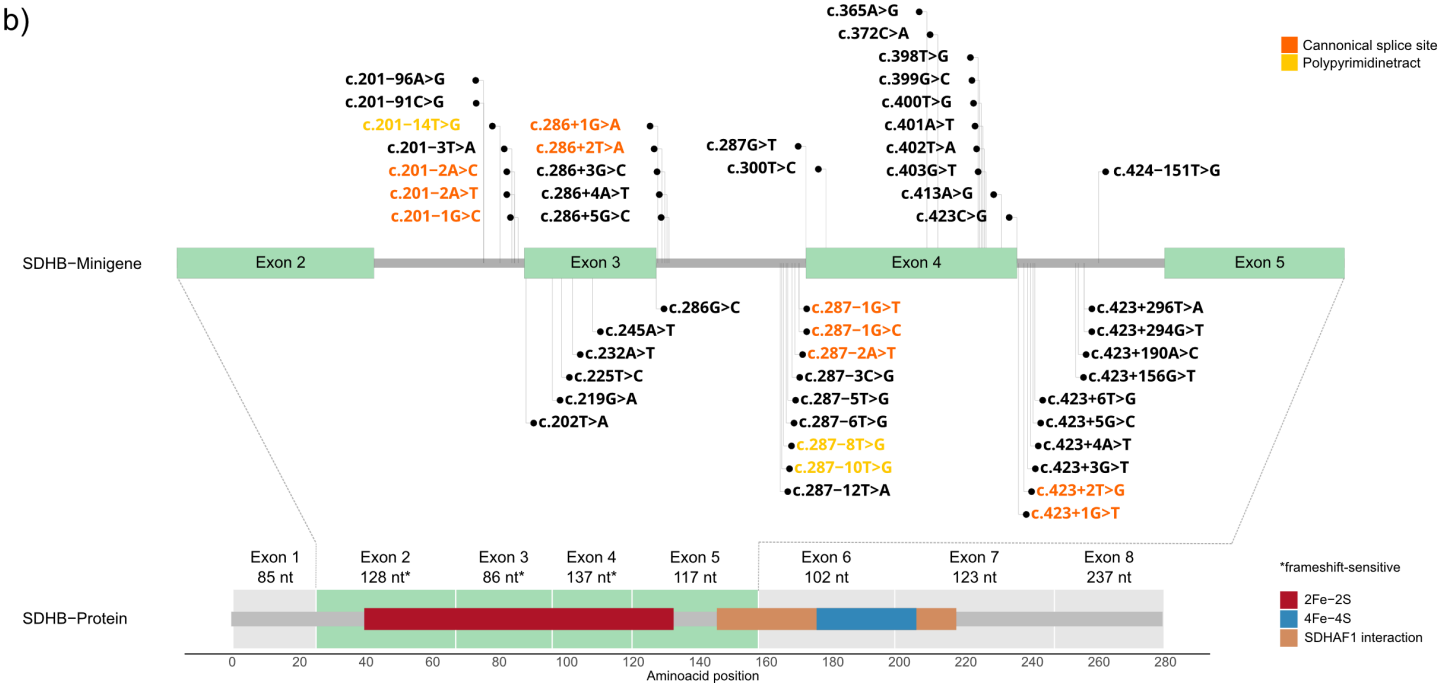


Figure 2

Figure 1. Workflow and variant selection to identify aberrant splicing of in-silico prioritized variants with an SDHB minigene of exons 2-5.

a) Workflow representing the SDHB minigene construction, variant prioritization, introduction of variants into the minigene, assessment of splicing with next generation sequencing (NGS) and variant reclassification. RT-PCR, Reverse transcription polymerase chain reaction. (Created in BioRender. Köhler, A. (2026))

b) Lollipop plot showing the distribution of 50 SDHB single nucleotide variants prioritized with SpliceAI and analyzed with the minigene comprising exons 2-5 and neighboring intronic sequences. The sequence is mapped to the SDHB transcript NM_003000.3 and annotated with exon numbers, amino acid positions and functional protein domains from UniProt P21912 reference. 2Fe-2S and 4Fe-4S refer to iron sulfur clusters. (Created with R.)



Figure 3

Figure 2. Experimental transcript outcomes and SpliceAI predictions for 50 *SDHB*variants.

Overview of the analyzed genomic regions (intron 2 to intron 4) with annotated splicing elements, including canonical splice sites (orange) and polypyrimidine tracts (yellow). The pre-assessment variant classification prior to integration of RNA evidence was indicated. ((L)P, likely pathogenic/pathogenic; VUS, variant of unknown significance; (L)B, likely benign/benign. Stacked bar plots show the distribution of transcripts assessed by minigene assay for each variant, ratios normalized to 1.0, classified as premature termination codon (PTC, red), full-length (teal), in-frame (yellow), or uncharacterized transcripts (purple). Variants were labeled using HGVS cDNA nomenclature and ordered by genomic position. The lower heatmap displays SpliceAI delta scores (AL, acceptor loss; AG, acceptor gain; DL, donor loss; DG, donor gain), with color intensity indicating predicted splicing impact. (Created with R)

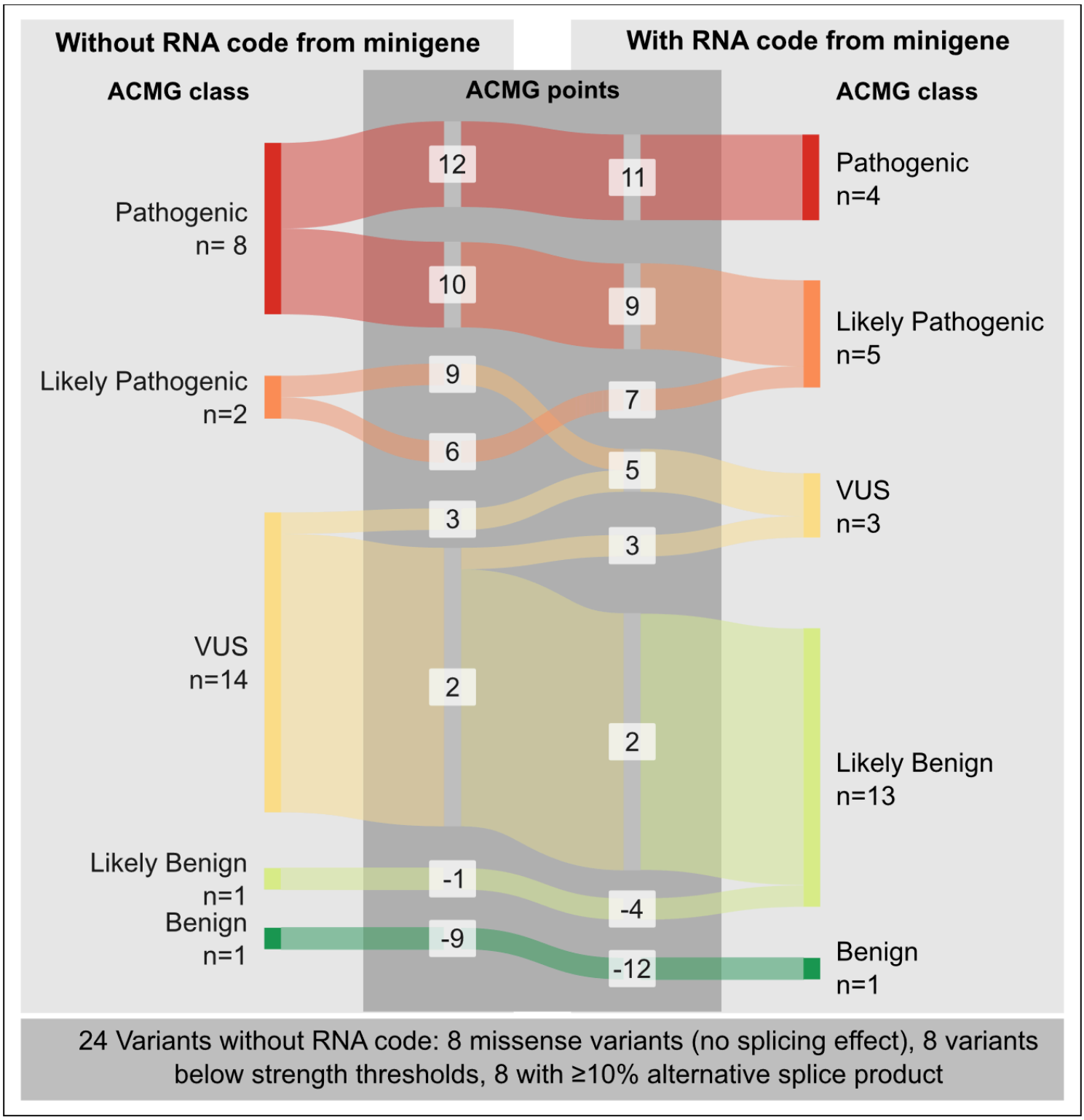


Figure 4

Figure 3. **Overview of point- and class-level changes before and after integrating RNA evidence.**(Diagram created using SankeyMATIC)

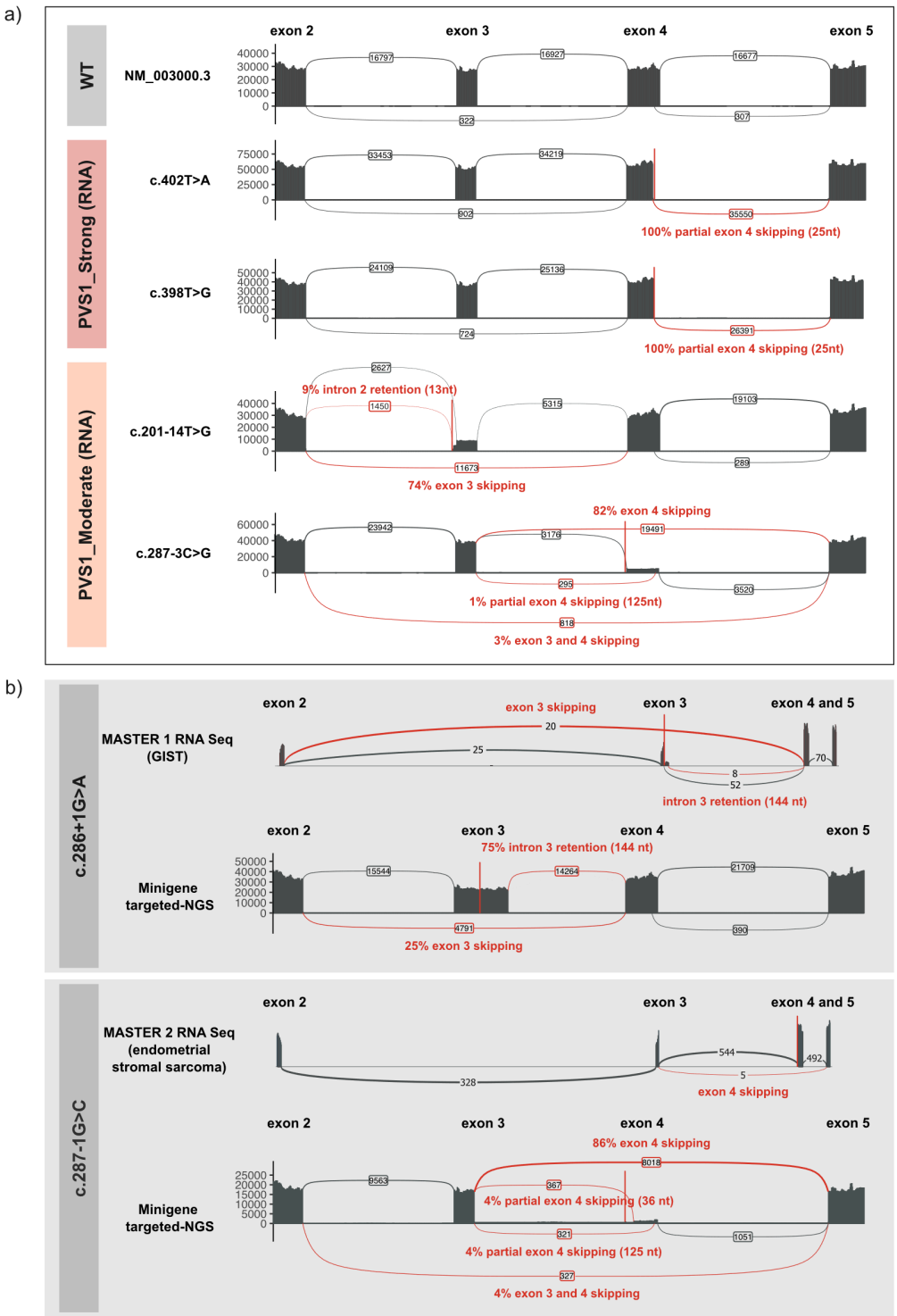


Figure 5

Figure 4. Sashimi plots and functional annotation of splice effects for selected SDHB variants

a) Sashimi plots of four selected variants showing aberrant splice patterns in the minigene assay, with aberrant transcripts highlighted in red and variant positions indicated by red vertical lines. Only uniquely mapping reads were included. Cut off for splice junction reads in the visualization was 1% (of max. read count). ACMG/AMP RNA evidence codes were assigned based on minigene-derived transcript proportions as follows: c.402T>A: 100% PVS1; c.398T>G: 100% PVS1; c.201-14T>G: 83% PVS1 and 17% BP7_S (full-length wildtype); c.287-3C>G: 86% PVS1 and 14% BP7_S (full-length wildtype).

b) Sashimi plots of two splice-altering variants compared with tumor RNA sequencing data from two affected patients of the NCT/DKTK/DKFZ MASTER program. Aberrant transcripts are highlighted in red, and variant positions are indicated by red vertical lines. Minigene-derived transcript proportions were used to assign ACMG/AMP RNA evidence codes as follows: c.286+1G>A: 100% PVS1; 287-1G>C: 93% PVS1, 4% PVS1_S and 4% N/A (total intron 3 retention). GIST, gastrointestinal stromal tumor.

Supplementary Files

This is a list of supplementary files associated with this preprint. Click to download.

- SDHBMinigeneSupplementalMaterial.pdf
- SDHBMinigeneSupplementalFigures.pdf
- SuppTab1SpliceAIprioritization.xlsx
- SuppTab2Splicejunctionanalysis.xlsx
- SuppTab3Transcriptanalysisresults.xlsx
- SuppTab4ExtentedTab1.xlsx